

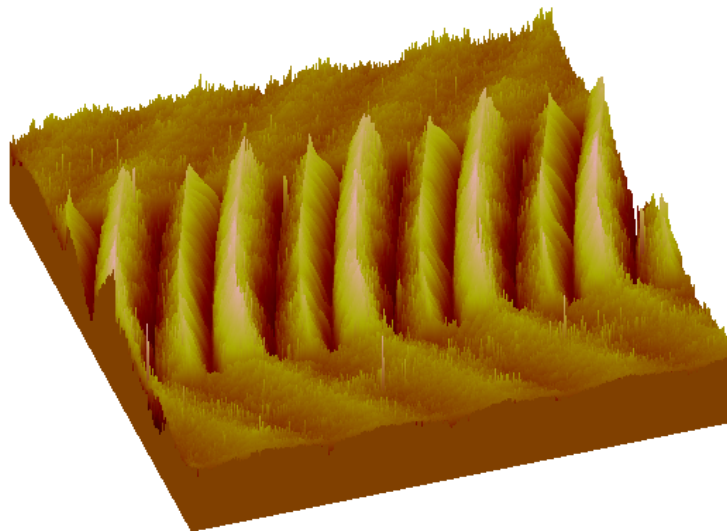
Characterization of piezo- and ferroelectric thin films by Scanning Probe Techniques

Master-thesis

R.J.A. Steenwelle

Enschede, 14 September 2007

Major subject: Applied Physics



Inorganic Materials Science
Faculty of Science & Technology
University of Twente

Summary

The aim of this thesis is to characterize the piezoelectric and ferroelectric properties of thin films, by scanning probe microscopy, in particular the quantitative measurement of the longitudinal piezoelectric constant. Due to the recent revival of interest in piezo- and ferroelectric thin films technology, simple and accurate techniques are needed. The rise of Scanning Probe Microscopy opens new possibilities for characterization of piezoelectric thin films. Two techniques have been explored: Piezo Force Microscopy, which cannot be used to obtain a reliable quantitative value of the longitudinal piezoelectric coefficient, and Piezo Scanning Tunneling Microscopy, which can be used to obtain reliable and accurate coefficients.

Piezo Force Microscopy is an Atomic Force Microscopy based technique which is able to image ferroelectric domain structure and locally polarize the ferroelectric surface, also called ferroelectric lithography. However it cannot give quantitative information on the magnitude of the piezoelectric coefficient, due to the inhomogeneous and not well-defined electric field in the material and complex tip-sample interactions.

Piezo Scanning Tunneling Microscope (PSTM) has great potential to become a new technique for quantitative determination of the longitudinal piezoelectric coefficient d_{33} . Scanning Tunneling Microscopy (STM) is available in most research laboratories and the PSTM technique is easy to implement on the STM. Since the tunneling current depends exponentially on the tip-sample distance, high sensitivity can be obtained. The possibilities of Piezo STM were explored on a PZT thin film grown on an STO substrate. Both top and bottom electrode are deposited, forming a capacitor with a well-known electric field in between. The PZT (52/48) thin films are grown on STO and all had a (001) orientation. The electrodes consist of epitaxially grown SRO. The method showed sensitivity down to 10 pm, under ideal conditions. Furthermore ferroelectric hysteresis loops could be acquired, plotting the piezoelectric deformation as a function of the applied voltage. An asymmetry in this piezoresponse was attributed to electrodes effects. Some external effects, for example electrical charging were discussed as well.

Finally, spectroscopic PSTM was used to determine the piezoelectric coefficient from the exponential decay of the tunneling current. By keeping the tip at a constant height and measure the tunneling current as a function the applied voltage, the piezoelectric coefficient can be calculated. However, more efforts are needed to improve the measurements and obtain piezoelectric coefficients that agree to expected values.

Contents

Introduction	4
Chapter 1 Theoretical background	6
1.1 Crystal structure	6
1.2 Dielectric materials	8
1.3 Piezoelectric materials	10
1.3.1 <i>Basics</i>	10
1.3.2 <i>Piezoelectricity in three dimensions</i>	11
1.3.3 <i>Constitutive equations and piezoelectric coefficients derived from thermodynamics</i> 13	
1.4 Ferroelectric materials	15
1.4.1 <i>Basics</i>	15
1.4.2 <i>Ferroelectric domain formation and hysteresis</i>	17
1.5 Piezoelectric and ferroelectric materials: properties and growth	18
Chapter 2 Sample fabrication and characterization	21
2.1 Configuration	21
2.2 Substrate	21
2.3 Pulsed Laser Deposition	21
2.4 Etching	23
2.5 Stencil deposition	23
2.6 Characterization of structure and composition	23
2.7 Wire bonding	23
Chapter 3 Piezo Force Microscopy	24
3.1 Principle of operation	24
3.2 Experimental	27
3.3 Results	29
3.3.1 <i>Regular PFM</i>	29
3.3.2 <i>Ferroelectric lithography</i>	30
3.3.3 <i>Local quantitative measurements by PFM</i>	31
3.3.4 <i>Modeling of the electric field</i>	32
3.3.5 <i>Cantilever-sample interaction</i>	33
3.3.6 <i>Probes and degradation of the sample</i>	35
Chapter 4 Piezoresponse Scanning Tunneling Microscopy (PSTM)	38
4.1 Sample configuration	38
4.2 Scanning Tunneling Microscopy	38
4.3 Principle of operation	39
4.4 Experimental	41
4.5 Results	43
4.5.1 <i>Topography STM</i>	43
4.5.2 <i>Macroscopic polarization measurements</i>	44
4.5.3 <i>PSTM measurements</i>	44
4.5.4 <i>Effects in the PSTM measurements</i>	46
4.6 Spectroscopic PSTM	50
4.6.1 <i>Principle of operation</i>	50
4.6.2 <i>Experimental setup</i>	52
4.6.3 <i>Results</i>	53

Conclusions and recommendations	55
Dankwoord	57
References	58

Cover: 3D-surface topography with piezoelectric surface deformations made by Scanning Tunneling Microscopy. At the top and bottom, the displacements are generated by a voltage of 0.5 V and have a magnitude of 50 pm. At the center the voltage is 6 V and magnitude is 1.3 nm. Frequency doubling occurs above the coercive voltage and is caused by ferroelectric switching.

Graduation committee:

Chairman

Prof. Dr. Ing. D.H.A. Blank

Members

Prof. Dr. Ir. H.J.W. Zandvliet

Dr. Ing. A.J.H.M. Rijnders

Ir. P.M. Te Riele

Introduction

Piezoelectric materials are materials that deform when a voltage is applied to it, and vice versa. They can be used wherever a displacement needs to be converted into an electrical voltage, for example sensors, generators (e.g. igniter), control panels (touch screens) or switches. Vice versa, a voltage can be converted to a displacement, for example micro- and nanoactuators, ultrasound transducers (e.g. medical equipment, and sonar), speakers (mobile phones), electronic components (bulk acoustic waves, surface acoustic waves). Some piezoelectric materials are also ferroelectric, which means the polarization can be switched. This memory-effect can be used in Ferroelectric Random Access Memories (FRAM).

The combination of piezoelectric materials and thin films technology has revived interest in research of ferroelectric and piezoelectric materials. The control of functional properties of piezoelectric and ferroelectric materials at decreasing length-scales can open up possibilities to build new 'smart devices'.

Characterization of piezoelectric thin films with high accuracy and reliability is essential to understand all important phenomena for these materials. A variety of methods have been developed for electrical, mechanical and thermal investigation. Especially the quantitative measurement of the mechanical response of piezoelectric thin films is important, but only few methods show a longitudinal resolution down to the sub-nanoscale. For example, optical methods such as interferometry have been used for sub-Angstrom deformation measurements, but still need large areas for analyses.

Scanning Probe Microscopy (SPM) has developed into an important analysis tool in materials science in the last two decades. It uses a physical probe to scan a surface in real space so the resolution is not limited by diffraction in reciprocal space. The rise of SPM provided new possibilities to analyze piezoelectric response of surfaces, using Piezo Force Microscopy or Piezo Response Atomic Force Microscopy. This technique is based on contact-mode Atomic Force Microscopy where a conductive tip induces piezoelectric deformations in the sample and measures these deformations simultaneously. The use of lock-in technique allows for detection of phase and amplitude data through the AFM tip-deflection. In this way local information of piezoelectric properties such as the domain structures can be acquired, by imaging static and dynamic polarization of ferroelectric films. However, this technique cannot detect the exact value of the amplitude of the piezoelectric deformation, which is very important in quantification of piezoelectric thin films.

Scanning Tunneling Microscopy may be a method to quantitatively obtain reliable results of piezoelectric deformations of thin films, with high resolution. The Piezoresponse Scanning Tunneling Microscopy has not been widely used yet, although it shows potential to become a great alternative to methods mentioned above. The piezoresponse measurements can be easily implemented on standard Scanning Tunneling Microscopes, which are widely present in research groups. The technique still needs exploration, such as the search for optimum operation conditions, the limitations to resolution and reliability of results.

The aim of the work described in this report is to explore techniques that were mentioned above. Piezo Force Microscopy is investigated, to study the possibilities for quantitative measurement of the piezoelectric constant. A study into the intrinsic principle of signal-formation and the consequences of the PFM-tip are presented. Subsequently the focus is shifted to Piezo Scanning Tunneling Microscopy, to study its possibilities for quantitative measurement of the piezoelectric constant. Questions that this study will focus on are: what is the minimal detectable deformation and piezoelectric constant, how do the results reflect physical phenomena like piezoelectricity and ferroelectricity, what are the operating conditions and what external effects can degrade the measurements. Finally an STM operating in spectroscopic mode has been explored for measurement of the piezoelectric constant.

The outline of the report is as follows. First a theoretical survey of dielectric, piezoelectric and ferroelectric materials is presented, followed by an investigation of the material $\text{Pb}(\text{Zr}_x\text{Ti}_{1-x})\text{O}_3$ (PZT). This material is currently the most widely used in piezoelectric applications. Two Scanning Probe Techniques are presented

afterwards, Piezo Force Microscopy and Piezoresponse Scanning Tunneling Microscopy. For both techniques the basic principles, experimental conditions and results will be discussed.

Chapter 1 Theoretical background

This chapter will study the dielectric, piezoelectric and ferroelectric materials and their properties. Furthermore these classes of these materials are mutually related in their properties by their crystal structure and symmetry and this will be described as well.

1.1 Crystal structure

All physical substances can be categorized according to their electrical conductivity, into, amongst others conductors, semiconductors and insulators. A material is electrically insulating when electrons are bound to their molecules. Insulating materials are also called dielectric, since for most insulating materials an applied electrical field can redistribute the electrons in such a way that the resulting polarization varies approximately linearly with the electric field. Another qualification of physical solids can be made on basis of their crystallinity. When atoms, molecules or ions are packed in a regularly ordered repeating pattern, materials are called crystalline. Materials are called single crystalline when the crystal lattice of the entire sample is continuous, with no grain boundaries or dislocations. The opposite of a single crystal sample is a polycrystalline sample, which is made up of a number of smaller crystals known as crystallites.

A number of special electrical phenomena can occur in dielectric crystalline materials. Several subclasses of dielectric materials can be recognized on basis of these phenomena

- Piezoelectric: Materials that generate an electrical potential in response to an applied stress.
- Pyroelectric: Materials that generate an electrical potential when they are heated or cooled.
- Ferroelectric: Materials where the spontaneous polarization can be reversed by applying an electric field.

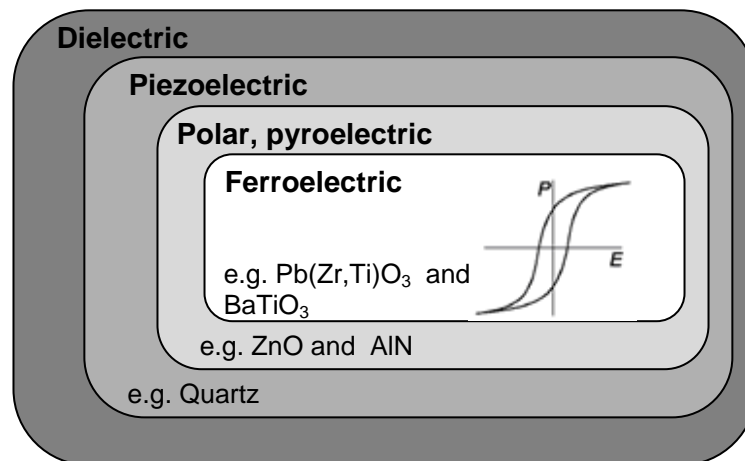


Figure 1-1 Schematic representation of ferroelectric, pyroelectric and piezoelectric materials

Figure 1-1 shows the subdivision of several groups of dielectric materials. For example it is shown that all ferroelectrics are piezoelectric, but not all piezoelectrics are ferroelectric. It should also be noted that some ferroelectrics show a very small piezoelectric effect. The class of pyroelectric materials will not be discussed further in this thesis.

In these dielectrics, a dipole is generated by a shift of charge inside the crystal lattice or a distortion of the crystal. The polarization of a dielectric material can interact with the crystal in a number of ways. This can be explained by structure and symmetry of the crystalline system¹. Performing a single symmetry operation leaves the crystal unchanged. Macroscopic symmetry elements in crystals are a center of symmetry, mirror

plane, 1-, 2-, 3-, 4- or 6- fold rotation axes and 1-, 2-, 3-, 4- or 6- fold inversion axes. A combination of these symmetry elements gives us the macroscopic symmetry also called as point groups.

Crystals can be classified into 32 point groups according to their crystallographic symmetry, and these point groups can be divided into two classes: one with a center of symmetry and one without a center of symmetry. Furthermore the non centro symmetric point groups can be split into groups with a unique polarization axis and ones without a polarization axis. Finally the polar Figure 1-2 shows the classification of dielectrics according to the presence a center of symmetry and a polar axis.

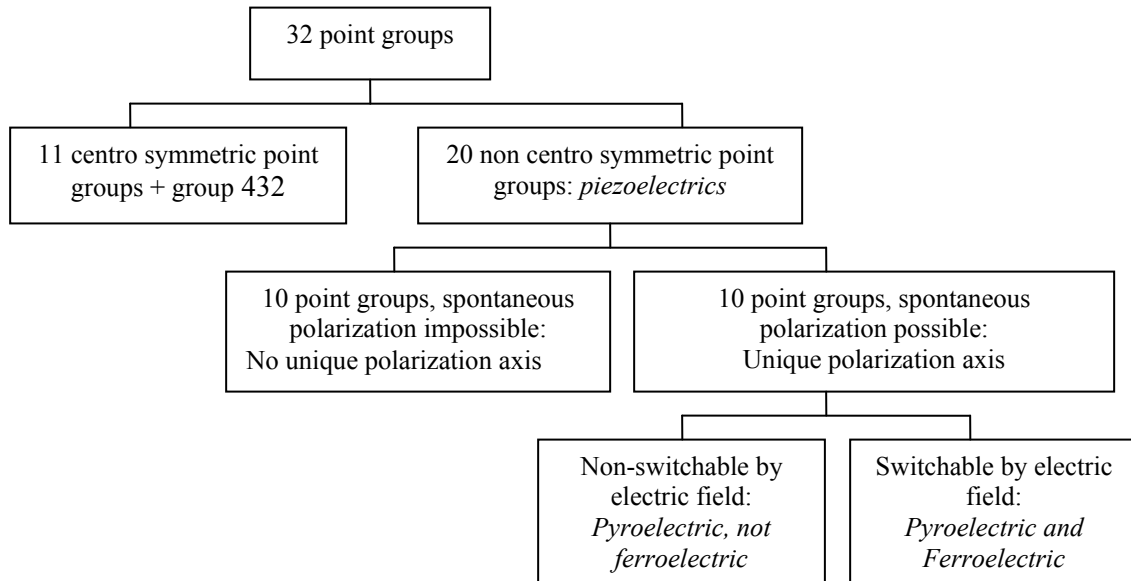


Figure 1-2 Classification of point groups

Figure 1-3 gives an indication of these two properties in a 2D crystal. A centro symmetric crystal cannot be polar, since a symmetry operation would invert the polarization vector and change the crystal. Non-centro symmetric materials can become polar, in the sense that there is a net dipole moment, depending on certain conditions. For example, all non-centro symmetric materials, except the 432 point group, have the ability to develop a polarization proportional to a strain. Therefore these materials are called piezoelectrics.

Furthermore, the class of non centro symmetric point groups can be divided into a class for materials that can possess a spontaneous polarization and a class for materials that cannot have it. Spontaneous polarization means a polarization exists even in absence of an external electric field or mechanical stress. Materials can have a spontaneous polarization if they possess a unique polar axis which macroscopically generates a polarization. For materials without spontaneous polarization more than one axis or no axes at all may be present. These are called pyroelectric, since polarization state may vanish when heated above its transition temperature. By the way, in pyroelectrics, the spontaneous polarization can be responsible for the piezoelectricity. These materials will lose its piezoelectric effect, when heated above the pyroelectric transition temperature. Other materials still exhibit piezoelectricity when heated above the transition temperature, since polarization may be caused by the non centro symmetry of the crystal as well.²

The class of pyroelectrics can be divided into a class of materials which can be switched between stable states of spontaneous polarizations by an external electric field and a class of materials which cannot be switched.

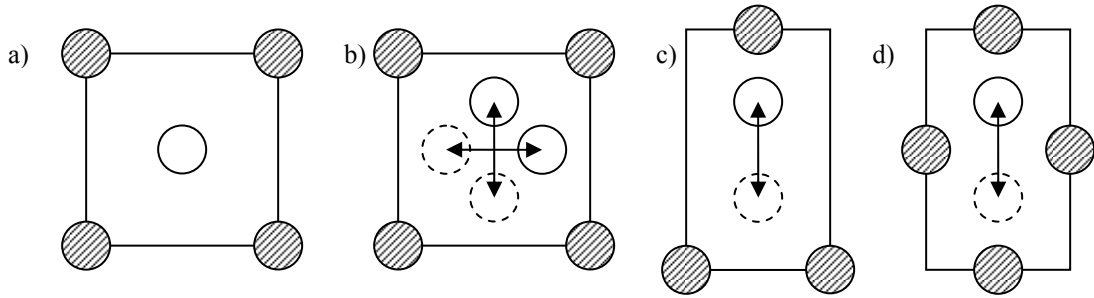


Figure 1-3 Examples of unit-cells in two dimensions with a) centro symmetry b) non centro symmetry with no unique polar axis, c) non centro symmetry with unique polarization axis with c) non centro symmetry with non-switchable polarization state (pyroelectric), and d) non centro symmetric with two switchable polarizations (ferroelectric)

In the following paragraphs a deeper look will be given into the dielectric, piezoelectric and ferroelectric materials.

1.2 Dielectric materials

Dielectric materials are insulating solids that can be polarized. The movement of charge within an atom or molecule generates an electrical dipole on a molecular or atomic level. Polarization is the alignment of dipole moments in the presence of an externally applied electric field. The electric dipole consists of two charges of equal magnitude but of opposite sign separated over a distance d . The electric dipole moment of this configuration is defined by the vector \vec{p} directed from $-q$ to $+q$ along the line between the charges:

$$\vec{p} = q \cdot \vec{d} \quad (1.1)$$

There are three microscopic origins of polarization: electronic, ionic and orientation, see Figure 1-4. The electronic polarization is a shift of the electron cloud relative to the nucleus. The ionic polarization is the shift of ions in their crystal lattice. The rotational polarization is associated with the rotation of permanent dipole, for example in liquids. Also mobile charge carriers in the form of ions or electrons can migrate under applied fields. Measurement of the polarization as a function of frequency can separate the mechanisms, since each mechanism is associated a maximum characteristic frequency.³

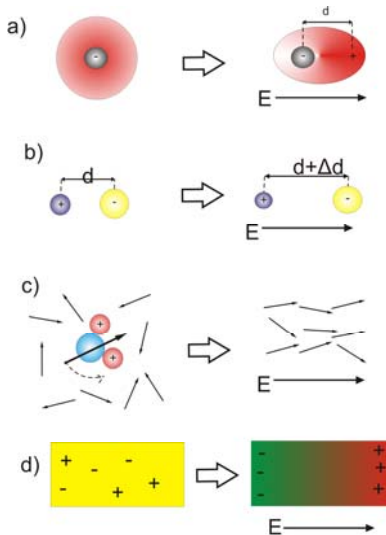


Figure 1-4 Polarization mechanism in dielectrics a) Electronic polarization, shift of electron cloud relative to the nucleus, b) Ionic polarization, change of ionic distance, c) Orientational, rotational alignment of permanent dipoles, d) Polarization of mobile charge carriers⁴

The intrinsic origin of polarization is based on forces existing between charges. It can be described from Coulomb's law $\vec{F} = \frac{1}{4\pi\epsilon_0} \frac{qQ}{r^2} \hat{r}$ and the definition of the electric field $\vec{F} = Q \cdot \vec{E}$. Polar molecules in an electric field will feel a force $\vec{F} = (\vec{p} \cdot \nabla) \vec{E}$ and a torque $\vec{N} = \vec{p} \times \vec{E}$. Therefore when an external field is applied, the atomic or molecular dipole moments will align to the field direction.

The total macroscopic polarization \vec{P} is defined as the dipole moment per unit volume. Each of the origins of the polarization can be integrated over the volume

$$\vec{P} = \frac{1}{V} \iiint_V \vec{p} dV \quad (1.2)$$

Generally dielectrics are described using a linear relationship between the external applied field \vec{E}_{ex} and the resulting polarization \vec{P} :

$$\vec{P} = \epsilon_0 \chi \vec{E} \quad (1.3)$$

Often the linear relationship between and the electrical displacement \vec{D} , related by the dielectric constant ϵ_r :

$$\vec{D} = \epsilon_r \epsilon_0 \vec{E}_{ex} \quad (1.4)$$

The electrical displacement \vec{D} inside a medium is the sum of two contributions: the external field \vec{E}_{ex} in vacuum, and polarization of the material \vec{P} , that is generated by the external field⁵:

$$\vec{D} = \epsilon_0 \vec{E}_{ex} + \vec{P} \quad (1.5)$$

$$\vec{D} = \epsilon_0 \vec{E}_{ex} + \epsilon_0 \chi \vec{E}_{ex} \quad (1.6)$$

The permittivity is defined by relative dielectric constant ϵ_r and the permittivity of free space ϵ_0 :

$$\epsilon_r \epsilon_0 \equiv \epsilon_0 + \epsilon_0 \chi = \epsilon_0 (1 + \chi) \quad (1.7)$$

The relative dielectric constant and the dielectric susceptibility are related by:

$$\epsilon_r = 1 + \chi \quad (1.8)$$

An analog description of linear dielectrics uses the induced charges, which are generated by an external E-field. Two types of induced charges will be generated: a surface charge $\sigma_b = \vec{P} \cdot \vec{n}$, where \vec{P} is the

polarization vector and \vec{n} is the normal vector to the surface, and a bound charge $\rho_b = -\nabla \cdot \vec{P}$, which is the divergence of the polarization vector. Most ceramic materials have dielectric constants within the range of 5-10. However titanate based ceramics (such as BaTiO₃ and PZT) can exhibit very high dielectric constants, in the order of a thousand. It should be noted that the frequency of the external field is important in determining the dielectric constant.

1.3 Piezoelectric materials

1.3.1 Basics

Piezoelectric materials generate charges under an applied stress (direct piezoelectric effect) and show a deformation under an applied voltage (inverse piezoelectric effect). The word ‘piezo’ is derived from the Greek *piezein*, which means to squeeze or press. In 1880 the Curie brothers found that quartz changed its dimensions when subjected to an electric field and conversely generated an electric charge when it was pressed⁶.

The linear relationship between the applied stress X and the resulting polarization P :

$$P = d^{direct} \cdot X \quad (1.9)$$

and d^{direct} is the piezoelectric coefficient.

Vice versa, when an external electric field E is applied to a crystal, this can cause a strain x in the material. This results in a physical contraction or expansion of the sample (see figure 1-5). This phenomenon is called the inverse piezoelectric effect:

$$x = d^{inverse} \cdot E \quad (1.10)$$

The piezoelectric constant d^{direct} can be expressed as a measured in Coulomb per Newton [C/N] for the inverse piezoelectric coefficient $d^{inverse}$ and meter per Volt [m/V]. Typical sizes for useful piezoelectric materials range from about 1 pm/V for quartz materials to about 1000 pm/V for PZT ceramics³.

In a realistic situation, a piezoelectric thin film consists of a top electrode, a bottom electrode and the piezoelectric material in between, see Figure 1-5. This situation can be thought of as an ideal capacitor, if electrode area A is bigger than the dielectric medium d ($A \gg d$). A voltage is applied between the top and bottom electrode and generates an electrical field in the medium. The electrical field is:

$$E = \frac{V}{d} \quad (1.11)$$

For a piezoelectric medium, the sample deformation will be perpendicular to the top electrode. Using the deformation-strain relation equation 1.8, and the strain as a function of the deformation:

$$x = \frac{\Delta z}{d} \quad (1.12)$$

The following direct relation between piezoelectric deformation Δz and the applied voltage can be obtained:

$$\Delta z = d_{33} \cdot V \quad (1.13)$$

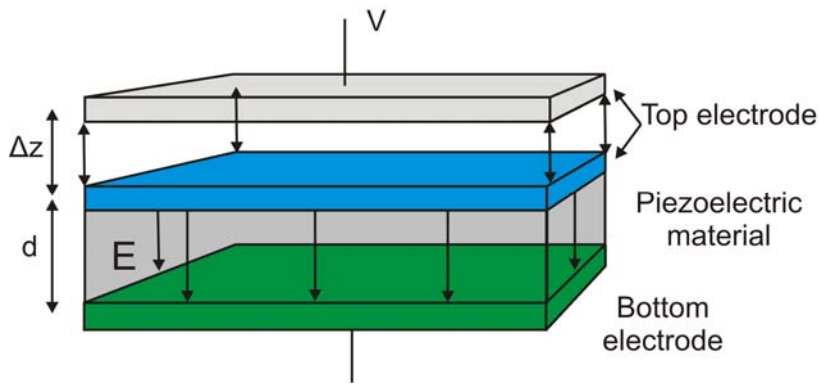


Figure 1-5 Configuration of a piezoelectric sample. An electric field is generated between the top and bottom electrode. A deformation Δz of the sample will occur.

The piezoelectric deformation Δz shows a linear relation to the voltage and is independent of the thickness of the piezoelectric layer. It should be noted that although the piezoelectric deformation is, in principle, directly related to the electric field, in the ideal capacitor approximation the electric field is directly dependant on the applied voltage and that the voltage may be the input to calculate the piezoelectric deformation.

The subscripts of the piezoelectric coefficient denominate the direction of the input electric field and the resulting deformation, which are in this case both out-of-plane. The d_{33} , or longitudinal piezoelectric coefficient, represents a deformation of the sample along the out-of-plane direction when the applied field is in the same direction. The d_{31} , or transverse piezoelectric coefficient, represents an expansion or contraction of the sample in the direction perpendicular to the applied field. The d_{15} coefficient describes shear deformation of the ferroelectric sample. More on directional piezoelectricity in paragraph 1.3.2.

The piezoelectric displacement can be plotted as a function of voltage. Figure 1-6a shows a purely piezoelectric response, linear as a function of the voltage. Figure 1-6b shows a piezoelectric with a ferroelectric switching effect. At a certain coercive voltage, the polarization suddenly switches in direction. This reversal of the polarization will also generate a sudden reversal of the physical deformation of the material and thus the piezoelectric coefficient changes sign. Moreover, a hysteresis loop is obtained, which is usually called the piezoelectric ‘butterfly loop’, obviously named after its shape. Usually the first cycle will form start at zero and converge to the hysteresis loop. The ferroelectric effect will be explained in paragraph 1-4.

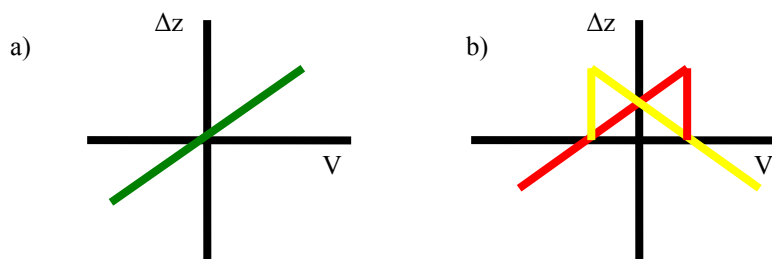


Figure 1-6 a) Linear piezoelectric behavior b) ‘Butterfly loop’ in strain $x(=\delta l/l)$ vs. voltage V , describing the response of a piezo actuator to a bipolar drive voltage. When a certain threshold voltage (negative to the polarization direction) is exceeded, reversion of polarization can occur.

1.3.2 Piezoelectricity in three dimensions

In reality the piezoelectric effect is strongly dependent on the direction. The piezoelectric effect always has a response in several directions. In case of a c-axis oriented PZT and an applied electric field in this direction, the out-of-plane piezoelectric response d_{33} will be used. This is the most simplified approach, since several other configurations other directions are evenly important. To make a coupling from the 1-

dimensional piezoelectric effect to a 3-dimensional approach, a simple mathematical framework can be used.

A realistic description uses a piezoelectric coefficient that is a 3rd rank piezoelectric tensor, based on the principal crystallographic axes. In case of the indirect piezoelectric effect it is:

$$x_{ij} = d_{kij}^{inverse} E_k \quad (1.14)$$

The 27 tensor-coefficients d_{kij} couple the input and output parameters. Input parameter is the electric field in direction $k=1,2$ or 3. The strain refers to a fractional change of shape u_i in direction Z_i , in directions $i=1,2$ or 3, and $j=1,2$ or 3. This can be seen in Figure 1-7. Since strain is symmetric ($x_{ij}=x_{ji}$), the tensor can have components that are not independent, and thus represent the same stress or strain relations. These components can be eliminated, leaving 18 non-zero components. Using equation 1.12, the piezoelectric response in any direction can be calculated now, using tensor transformations.

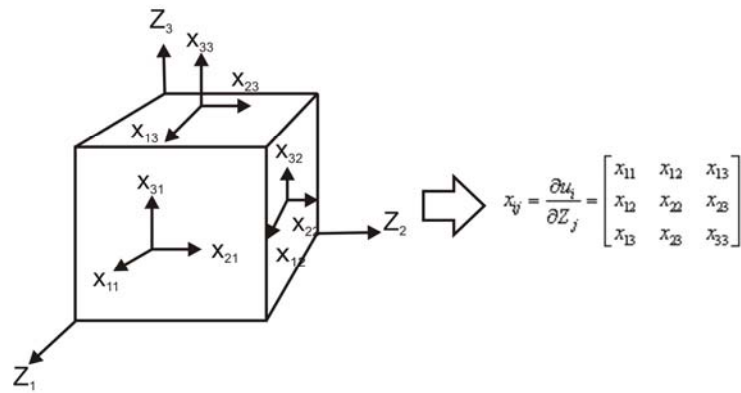


Figure 1-7 Strain represented by a 9-element matrix. Stress in all three directions are applied to three pairs of cube-faces.

To simplify the framework, index abbreviations can turn the tensor expression into a matrix expression. Since the stress or strain are symmetric indices, as was described above, they are rewritten, using $11 \rightarrow 1$, $22 \rightarrow 2$, $33 \rightarrow 3$. The mixed pairs of indices represent the shear deformation planes 23 or $32 \rightarrow 4$, 13 or $31 \rightarrow 5$, 12 or $21 \rightarrow 6$, resulting in the following matrix:

$$\begin{bmatrix} x_1 \\ x_2 \\ x_3 \\ x_4 \\ x_5 \\ x_6 \end{bmatrix} = \begin{pmatrix} d_{11} & d_{21} & d_{31} \\ d_{12} & d_{22} & d_{32} \\ d_{13} & d_{23} & d_{33} \\ d_{14} & d_{24} & d_{34} \\ d_{15} & d_{25} & d_{35} \\ d_{16} & d_{26} & d_{36} \end{pmatrix} \begin{bmatrix} E_1 \\ E_2 \\ E_3 \end{bmatrix} \quad (1.15)$$

Often experiments using the inverse piezoelectric effect, will use an electric field that is applied in the z -direction and the piezoresponse that will be either parallel or perpendicular to the applied field. Effectively only the longitudinal coefficient d_{33} , the transverse coefficient d_{31} , and the shear coefficient d_{31} can describe the total generated strain. The following matrix is constructed, where the zero superscript means that the value of the d_{33} , d_{31} and d_{15} are placed into the matrix. This is can only be done for tetragonal single crystals and this reduction is only valid when the crystallographic axes are orthogonal and the input and output is parallel to these axes. If this is not the case, the piezoresponse matrix becomes very complex.

$$d_{ki}^0 = \begin{pmatrix} 0 & 0 & d_{31}^0 \\ 0 & 0 & d_{31}^0 \\ 0 & 0 & d_{33}^0 \\ 0 & d_{15}^0 & 0 \\ d_{15}^0 & 0 & 0 \\ 0 & 0 & 0 \end{pmatrix} \quad (1.16)$$

The piezoelectric activity can be observed as a surface in 3D, by Harnagea⁷ for tetragonal PZT and BaTiO₃, and using more complex calculations, for rhombohedral PZT, Figure 1-8. The imaginable vector from the origin to an intercept of this vector with the surface determines the magnitude of the longitudinal piezoelectric coefficient in that direction. These images represent an arbitrary rotation of the crystal orientation in three dimensions, after which the d_{33} calculated.

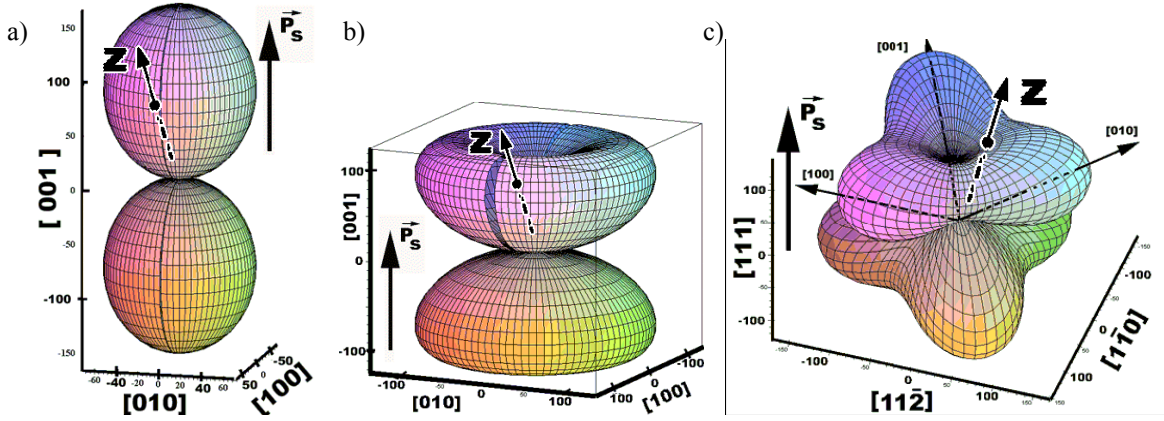


Figure 1-8 Longitudinal piezoelectric constant d_{33} for a) tetragonal PZT (40/60), b) BaTiO₃ and rhombohedral PZT⁷

1.3.3 Constitutive equations and piezoelectric coefficients derived from thermodynamics

Up to this point, only the applied electric field was coupled to the strain of a material by the direct and inverse piezoelectric effect (equation 1.9 and 1.10) and to the electrical displacement by the dielectric polarization (equation 1.3 and 1.4). In reality far more physical parameters are mutually influencing each other. To describe these thermal, electrical and mechanical effects, a thermodynamical framework can be used to derive the so-called coupled equations, which can be useful to interpret these interactions.

It is possible to describe the important features of ferroelectric materials without taking into account the microscopic mechanisms of ferroelectricity⁷. The elastic Gibbs free energy function should be used in most experimental situations, under isothermal conditions, with variables elastic strain x , external electric field E and internal energy U , entropy S and the independent variables electric displacement D , temperature T and elastic strain X :

$$G(T, X, D) = U - TS - X_{ij}x_{ij} \quad (1.17)$$

$$dG = -SdT - x_{ij}dX_{ij} + E_i dD_i \quad (1.18)$$

A stable ferroelectric phase follows from a given set of independent variables D , X and T for which the free energy is minimized. Expressions that relate dependent and independent variables may be obtained, using partial derivatives of the Gibbs energy to each of the independent variables⁸.

$$S = -\left[\frac{\partial G}{\partial T}\right]_{X=0, E=0}, x = -\left[\frac{\partial G}{\partial X}\right]_{E=0, T=0}, D = -\left[\frac{\partial G}{\partial E}\right]_{X=0, T=0} \quad (1.19)$$

The second-order partial derivatives of this equation all identify a physical effect⁹. The dielectric coefficient, two piezoelectric coefficients and the elastic compliance coefficient can be calculated.

Firstly, the dielectric constant is:

$$\varepsilon = -\left[\frac{\partial^2 G}{\partial E \partial E}\right]_{X=0, T=0} = \left[\frac{\partial D}{\partial E}\right]_{X=0, T=0} \quad (1.20)$$

Secondly, two kinds of piezoelectric equations can be derived:

$$d = \left(\frac{\partial^2 G}{\partial X \partial E}\right)_{T=0} = \left(\frac{\partial D}{\partial X}\right)_{T=0, E=0}, d' = \left(\frac{\partial^2 G}{\partial E \partial X}\right)_{T=0} = \left(\frac{\partial x}{\partial E}\right)_{T=0, X=0} \quad (1.21)$$

The first one represents electric displacement versus stress [C/N], the second d' represents strain versus electric field [m/V]. It turns out that these correspond to the direct and converse piezoelectric effects, respectively. The order of the differentiation is considered to have a different meaning when interchanged.

In transducer applications a high d' is desirable, since a voltages should be generated in response to a mechanical stress. In sensor applications however, the material should possess a high d value, since then an electrical displacement should be generated by a strain. The d' and d are related by the dielectric constant¹⁰:

$$d' = \frac{d}{\varepsilon_0 \varepsilon_r} \quad (1.22)$$

Elastic properties can be described using the above formalism as well. The elastic compliance is:

$$s = -\left[\frac{\partial^2 G}{\partial X \partial X}\right]_{E=0, T=0} = \left[\frac{\partial x}{\partial X}\right]_{E=0, T=0} = \frac{1}{c} \quad (1.23)$$

This expression represents a strain versus applied stress. It is also called the Young's modulus. The elastic compliance is the inverse of the elastic stiffness c , which is used in some cases. For the d' constant, the output is a force instead of a displacement. This constant describes the ability of the piezo to do work on a load, a property of the material that depends on the force generated by an applied voltage.

Several relations can be calculated to relate the above described coefficients, but these expressions will not be presented here. The physical phenomena described above may be combined into so-called coupled equations. The most widely used is the strain-charge form:¹¹

$$x = sX + dE \quad (1.24)$$

$$D = dX + \varepsilon E \quad (1.25)$$

When electric energy is supplied to a piezoelectric sample and some part is transduced into mechanical energy. The electromechanical coupling factor k is defined by the ratio of stored mechanical energy, which is determined by the strain x , and the input electrical energy, with s is the elastic compliance. The nominator is a measure of the mechanical energy, determined by the strain of the material. The denominator is a measure of the electrical energy and d is the inverse piezoelectric coefficient:¹²

$$k^2 = \frac{\frac{1}{2}(x^2 / s)}{\frac{1}{2}(\epsilon_0 \epsilon_r E^2)} \quad (1.26)$$

$$= d^2 / s \epsilon_0 \epsilon_r \quad (1.27)$$

The electrical, mechanical and thermal effects can influence each other, since terms attributed to these three effects are summed in equation 1.5 and 1.6, to give the Gibbs potential. For example, stress and stain in piezoelectric materials can have a big influence on ferro- and piezoelectric properties. In general the piezoelectric coefficient decreases when the stress increases⁷. Primary origin of homogeneous film strain is lattice mismatch between the film and substrate.¹³ The substrate may also limit the bending and stressing of the single-crystal thin films. The clamping effect is well-known for its distorting influence on the piezoresponse, due to a strong coupling of the in-plane and out-of-plane deformations. If the crystal cannot expand freely in-plane, the expansion in the z direction will be limited. The following expression described the clamping of the piezoelectric coefficient d_{33} by the substrate⁷:

$$d_{33}^{clamped} = \frac{x_3}{E_3} = d_{33} - 2d_{31} \frac{S_{13}^E}{S_{11}^E + S_{12}^E} \quad (1.28)$$

With x_3 deformation of the unit-cell in the z -directions. S_{1k}^E is the elastic compliancy in three directions for input in-plane and a constant external electric field. Since in most materials $d_{31} < 0$ and $s_{13} < 0$, the measured coefficient in films is halve the value of unclamped materials. Therefore, the small values of the piezoelectric coefficients in films relative to the bulk ceramic values can be at least partly explained by the clamping effects of the substrate.

1.4 Ferroelectric materials

1.4.1 Basics

Ferroelectric materials are dielectric materials characterized by a reversible spontaneous polarization. The word ‘ferro’ comes from the analogy that exists with *ferromagnetic* materials, in which a material exhibits a permanent magnetic moment. It was used to describe the ferromagnetism that is found in iron. Ferromagnetism was already known when ferroelectricity was discovered in the late 1800s.

In perovskite crystal structures, polarization results from the displacement d of one type of ion with electrical charge q , relative to the crystal lattice. For example, in $\text{Pb}(\text{Zr,Ti})\text{O}_3$, the dipole moment is caused by the displacement of either the Ti^{4+} or Zr^{4+} cations relative to the centre of the oxygen octahedron around the cation.

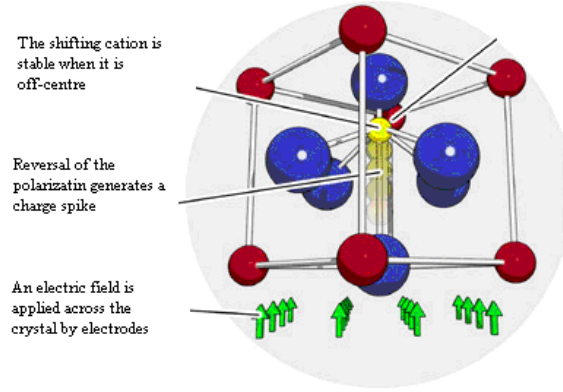


Figure 1-9 Switching a cation inside a PZT unit cell by applying a voltage over the material

The ferroelectricity adds a term to the electrical displacement equation:

$$\vec{D} = \epsilon_0 \vec{E} + \epsilon_0 \chi_0 \vec{E} + \vec{P}_s \quad (1.29)$$

Where \vec{P}_s is the spontaneous polarization.

Ferroelectrics can be explained theoretically by the phenomenological Ginzburg-Landau theory or by the macroscopic theory of soft-modes. Another simple observation of the stable minima occurring in ferroelectric materials can be given by reviewing the potential energy inside the crystal.¹⁰ Ions will shift and stabilize in a position that minimizes the energy. The force of the local electric fields due to the ions in the crystal increases faster than the elastic restoring forces. This leads to an asymmetrical shift in the equilibrium ion positions and hence to a permanent dipole moment.

$$E_{loc} = E_0 + \sum_i \frac{[3(\vec{p}_i \cdot \vec{r}_i) \vec{r}_i - r_i^2 \vec{p}_i]}{4\pi\epsilon_0 r_i^3} \quad (1.30)$$

$$E_{loc} = (\gamma / 3\epsilon_0) \vec{P} \quad (1.31)$$

Here γ is called the Lorentz factor. For an isotropic cubic system, it is known that $\gamma=1$ ¹⁴. If the ionic polarizability is α , the dipole moment of the unit cell of this crystal is:

$$\mu = (\alpha\gamma / 3\epsilon_0) \vec{P} \quad (1.32)$$

The energy of this dipole moment (dipole-dipole coupling) is:

$$W_{dip} = -N \mu \cdot E_{loc} = -(N\alpha\gamma^2 / 9\epsilon_0^2) \vec{P}^2 \quad (1.33)$$

With N is number of atoms per unit volume.

The elastic energy that counteracts the dipole interaction is:

$$W_{elas} = N[(k/2)\vec{u}^2 + (k'/4)\vec{u}^4] \quad (1.34)$$

With k and k' being the force constants and \vec{u} the displacement, this results in the expression for the total energy (using $\vec{P} = Nq\vec{u}$):

$$W_{tot} = W_{dip} + W_{elas} \quad (1.35)$$

$$W_{tot} = [(k/2Nq^2) - N\alpha\gamma^2/9\epsilon_0^2]\vec{P}^2 + (k'/4N^3q^4)\vec{P}^4 \quad (1.36)$$

From this, one can see that if the coefficient of the harmonic term of the elastic energy is equal to or greater than the coefficient of the dipole-dipole coupling, then $P=0$. Otherwise a shift from the equilibrium position is stable (see Figure 1-10). The Lorentz factor for perovskites is $\gamma \sim 10^2$, which is higher than for other crystal structures.

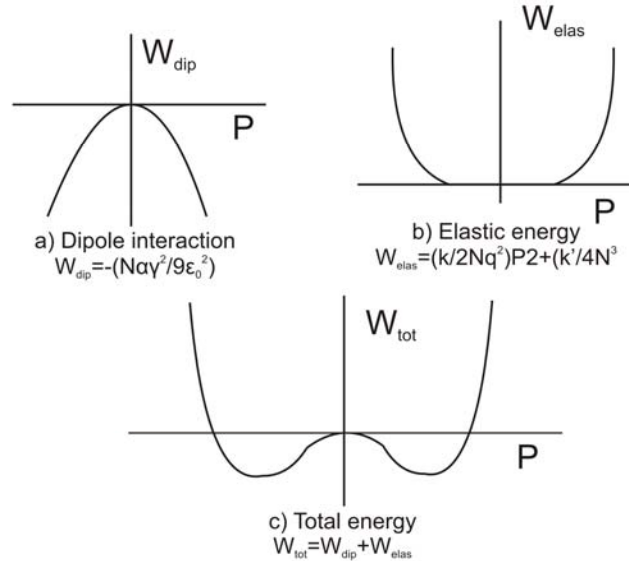


Figure 1-10 Energy explanation of spontaneous polarization

Most ferroelectric materials undergo a phase transition from a high-temperature nonferroelectric (or paraelectric) phase into a low-temperature ferroelectric phase, of lower crystal symmetry. The phase transition temperature is called the Curie temperature (T_c). In most cases, the dielectric constant above this temperature obeys the Curie-Weiss law, $\epsilon = C(T - T_0)^{-1}$, where C is the Curie constant and T_0 the Curie temperature.

1.4.2 Ferroelectric domain formation and hysteresis

Dielectrics which are in the paraelectric state (when $T > T_c$) contain permanent dipoles which can be directed along any direction. If the material undergoes a phase transition to the ferroelectric state ($T < T_c$) the polarization of each unit cell occurs in one of three favored crystal direction. Adjacent dipoles tend to orient themselves in the same direction, which induces a spontaneous polarization. Regions of uniform polarization are called domains, separated by domain walls. In ferroelectric materials, the domain walls are extremely narrow, often not more than one or two lattice layers. In a natural state all domain are randomly

oriented (following the crystal axes) and the ferroelectric material has a zero net macroscopically polarization. Dipoles can be switched by applying an external electric field. In this way the domains grow or shrink. A macroscopic polarization is generated. Domain formation is driven by minimization of the electrostatic energy of the depolarizing field. A split into domains of opposite polarization is energetically favorable. A fall-off of the polarization at a grain boundary usually causes strong depolarizing fields in the order of 10 kV/cm. Therefore, grain boundaries are favorable for domain wall formation.

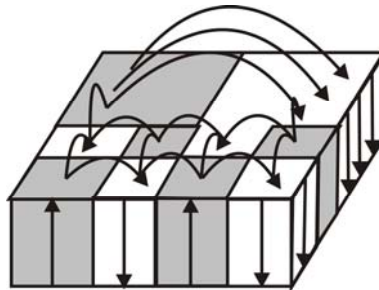


Figure 1-11 Depolarizing field and aligned dipoles: electric field lines show how a split of a domain can decrease the energy of the depolarizing field. For small domains the depolarizing fieldlines are smaller and are less energetic than the depolarizing fieldlines for large domains

The polarization behavior in an applied electric field is highly non-linear and exhibits a hysteresis loop due to switching of domains.

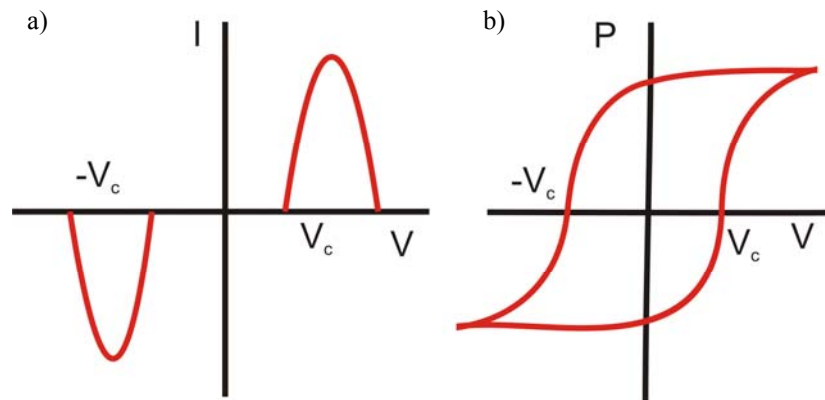


Figure 1-12 a) Current as a function of voltage graph and b) Polarization as a function of voltage, showing a hysteresis loop and coercive voltage V_c

In this figure the importance of the ‘history of net polarization’ of the material is visible. The remnant polarization is a measure of the remaining net electrical polarization, when the applied electrical field is removed. The coercive field is the electrical field necessary to drive the net electrical polarization back to zero in a material after being saturated, see Figure 1-12b. This happens in two directions of the applied field, thus for plus and minus the value of the coercive field. To describe the switching behavior in an ideal capacitor system, such as described in paragraph 1.3.1, the coercive voltage can be used, instead of the coercive field. The coercive field and coercive voltage are linearly related by the voltage by the thickness d of the layer, see also Equation 1.9.

Ferroelectric properties of materials are traditionally characterized by their I-V, see Figure 1-12a. From the charge transport that is measured at the electrodes, the polarization can be calculated. Important parameters are the applied voltage and the size of the electrodes of the sample, the dielectric constant and the leakage current of the material.

1.5 Piezoelectric and ferroelectric materials: properties and growth

This paragraph will describe the characteristics of bulk and thin film piezoelectric materials and thin films. After that focus will shift to Lead Zirconate Titanate ($\text{PbZr}_x\text{Ti}_{1-x}\text{O}_3$ or PZT), since that is the most used material in thin-films.

Bulk piezoelectric materials can be classified to have sample configurations thicker than typically $1\ \mu\text{m}$. Usually the bulk materials are ceramic, an inorganic non-metallic material whose formation is due to the action of heat. The fabrication process involves a powder of the proper composition is pressed into a solid. The resulting material has arbitrary aligned crystal and is isotropic. It does not show a piezoelectric effect, even for non centro symmetric crystals. To obtain piezoelectricity, the material needs to be poled. First the material is heated above its Curie transition temperature, where the material is in its tetragonal phase. During cooling down, the material is subjected to a large electric field. Below the Curie temperature the crystals will become ferroelectric again and align themselves along the electric field. Thus the permanent polarization and permanent deformation is ‘frozen’ into the material. The most widely used ceramic material in bulk is Lead Zirconate Titanate ($\text{PbZr}_x\text{Ti}_{1-x}\text{O}_3$ or PZT) used in standard piezo actuators, d_{33} is on the order of 450 to 650 pm/V and d_{31} is on the order of -200 to -300 pm/V. Another often used bulk ceramic is Barium Titanate (BaTiO_3).

Epitaxial thin-films are usually quasi-single-crystalline, meaning all crystals are perfectly aligned in the same direction next to each other on top of a carrier crystal. These materials offer large control of their properties, since they exhibit high degree of uniformity. The piezoelectric coefficients of these crystalline piezoelectric materials are in the order of 50 pm/V. It is lower than for bulk ceramic materials and a reason for this can be the high degree of ordering which restricts the deformation. The crystals are strongly related mutually causing an intrinsic clamping. Furthermore the thick substrate that is used for thin-films can also cause a significant clamping, see also paragraph 1.4.3 on this topic. Some natural single crystalline piezoelectric materials show even less piezoelectric activity, for example quartz (SiO_2) is 2 pm/V. Examples of piezoelectric materials that are used in thin-films are Aluminium Nitride (AlN), Zincite (ZnO), Lead Zirconate Titanate (PZT) and Barium Titanate (BaTiO_3) and Strontium Titanate (SrTiO_3).

A high piezoelectric coefficient is desirable for materials intended to develop motion or vibration, such as sonar or ultrasonic cleaner transducers. In a sample configuration that resembles a capacitor, the displacement of a piezo-active material can be estimated to be typically in the order of 0.1% of the thickness of the sample. Applying a larger voltage will cause electrical breakdown of the piezoelectric material.

Although there are a lot of piezoelectric materials interesting for applications, $\text{Pb}(\text{Zr}_x\text{Ti}_{1-x})\text{O}_3$ (PZT) is the material used in this report because of its high piezoelectric constant. PZT is a solid solution of PbTiO_3 and PbZrO_3 . Both materials and PZT are perovskites, all with a Curie temperature above room temperature.

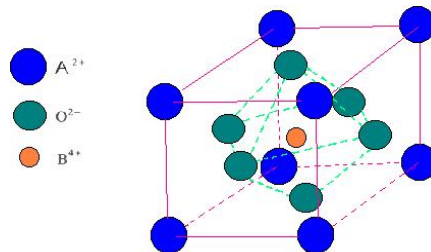


Figure 1-13 Crystal structure of a perovskite

Perovskites are a large family of crystalline ceramics that derive their name from a specific mineral known as perovskite. It consists of a cubic structure ABO_3 with the A-cation in the middle of the cube, the B-cation in the corner and the anion, commonly oxygen, in the centre of the face edges. The A and B atoms represent +2 and +4 ions respectively, or 3+ and 3+ ions respectively, while the O atom is the Oxygen⁻² ion. The perovskite structure can be found in many ferroelectrics, catalysts, sensors and superconductors.

PbTiO₃ is in a tetragonal ferroelectric phase, where the dipole moment in neighboring unit cells are aligned perpendicular in the 00l plane and PbZrO₃ is in an orthorhombic antiferroelectric phase, where the dipole moment in neighboring unit cells are aligned antiparallel in the 110 plane. Lattice parameters a=b of PbTiO₃ are 3.905 Å and PbZrO₃ is 4.159 Å.

The molar ratio x of Ti⁴⁺ ions to Zr⁴⁺ determines the phase of PZT, as can be seen in the phase diagram for PZT, Figure 1-14a. The solution features an extremely large dielectric constant and piezoelectric constant at the morphotropic phase boundary (MPB) near x = 0.52. PZT has a high polarization (=36 μC/cm²) and low coercive field (>20 kV/cm). These properties make PZT-based compounds one of the most prominent and useful in ferroelectric and piezoelectric applications. Figure 1-14b shows the effective piezoelectric coefficients for PZT ceramics as a function of composition, which were collected from a number of experiments.

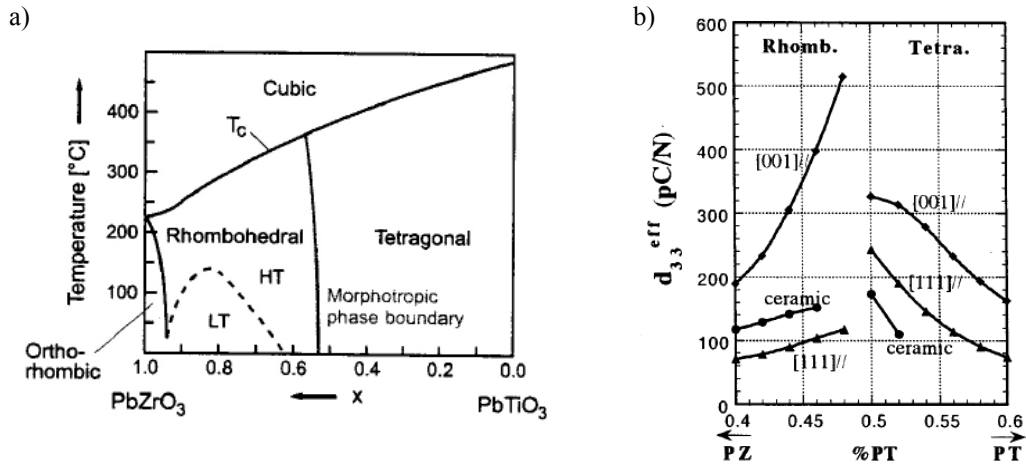


Figure 1-14 a) Phase diagram of PZT¹⁵ and b) d₃₃ as a function of the molar ratio Zr and Ti¹⁶

Deposition of PZT can be done by chemical vapor deposition (sol-gel, metal organic decomposition) or physical vapor deposition (sputtering, ion beam sputtering or pulsed laser ablation). In this work PLD has been used, which will be described in paragraph 2.3.

Chapter 2 Sample fabrication and characterization

This chapter will give an overview of the experimental techniques that were used to fabricate and characterize the samples.

2.1 Configuration

The sample configuration is shown in Figure 2-1. Strontium Rhutenate SrRO_3 (SRO) of 50 nm was deposited on the substrate of Strontium Titanate SrTiO_3 (STO), functioning as bottom electrode. Next the piezoelectric material Lead Zirconate Titanate $\text{Pb}(\text{Zr}_{0.52}\text{Ti}_{0.48})\text{O}_3$ (PZT) of 100 nm was deposited. For this composition the PZT is situated near the Morphotropic Phase Boundary, with a high piezoelectric constant. To make contact to the bottom electrode, the PZT was wet-etched on both sides. A bonding wire was placed to connect the bottom electrode to a conductive and magnetic nickel-plate, which was used as sample holder. For PSTM measurements an additional SRO top electrode was deposited by stencil deposition. Therefore it is indicated by a dotted line in Figure 2-1. All depositions were done by Pulsed Laser Deposition. More on every step will be described below.

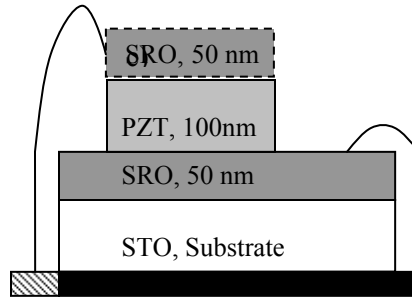


Figure 2-1 Schematic overview of the sample configuration in side view for the PFM measurements. The top SRO layer is dotted since it only is included for PSTM measurements.

2.2 Substrate

A Strontium Titanate single crystals were used as a substrate. It is an electrical insulating material, is mechanical stable and has a cubic perovskite structure with lattice parameter of 3.905 \AA at room temperature. To obtain a conducting bottom electrode, the substrate material can be doped with niobium to obtain a conductive substrate ($\text{Nb}:\text{SrTiO}_3$). However this has some disadvantages since the electrical behavior is semiconducting, in contrast to the preferred metallic behavior. Another option to obtain a suitable conductive layer is the deposition of a layer of half metallic SrRuO_3 on top of the SrTiO_3 substrate. This material has matching lattice parameters and has shown excellent properties as electrodes for PZT. At room temperature, it is an orthorhombic phase with lattice parameters $a = 5.5670 \text{ \AA}$, $b = 5.5304 \text{ \AA}$, and $c = 7.8446 \text{ \AA}$, but it can be considered as pseudo-cubic perovskite-like with $a = 3.930 \text{ \AA}$.¹⁷

2.3 Pulsed Laser Deposition

Pulsed Laser Deposition (PLD) is a physical vapor deposition technique. The deposition parameters are independently tunable and thus allowing an accurate control of deposition kinetics. Key features are a broad useable pressure range, stoichiometric transfer from the target to the film and a high deposition rate.

PLD is based on evaporation of material by an intense laser beam. The vaporized material forms a plume, and condenses on a substrate which is placed in the vacuum chamber opposite to the target. A thin film will form on this substrate. The thin film properties can be altered by process parameters or the type of substrate where the material is grown upon.

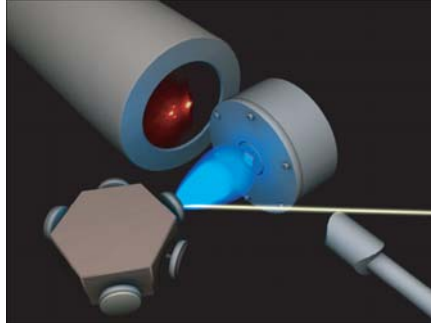


Figure 2-2 Schematic representation of the PLD process

The experimental set-up is schematically represented in Figure 2-2. The energy source is a KrF ($\lambda = 248$ nm) excimer laser (Lambda Physik, Compex 205) capable of operating at frequencies between 1-50 Hz. The pulse width is about 25 ns (FWHM) and the maximum pulse energy is 650 mJ. The laser pulse is focused onto the target under a 45° angle. The fluency and spot size mainly determines the amount of ablated material and determines whether stoichiometric ablation takes place. The gas pressure, substrate temperature and target-to-substrate distance influence the kinetic energy of the ablated material and therefore these are the most important parameters for controlling the deposition conditions. The used parameters are summarized in Table 2-1.

Table 2-1 Pulsed Laser Deposition parameters

	SrRuO ₃	Pb(Zr,Ti)O ₃
Laser energy density [J/cm ²]	2.5	2.5
Spot size [mm ²]	3.0	3.0
Pressure [gas; mbar]	0.13	0.10
Substrate Temperature [°C]	580	600
Laser frequency [Hz]	4	2
Target-to-substrate distance [mm]	58	58
Deposition rate [Å/pulse]	0.1	0.1

High substrate temperatures are necessary for epitaxial growth. Deposition temperature can be 250°C to 600°C, although low temperatures increase the need for post-deposition annealing to crystallize the film. Since lead or lead oxide compound is highly volatile at these temperatures, this imposes a maximum deposition temperature of 600°C.

The growth mechanism and crystal directions of the two interfaces (STO/SRO and SRO/PZT) have been investigated using techniques that will be described shortly. First, the deposition of SrRuO₃-film on (001) SrTiO₃ substrate was fully epitaxially. The crystal orientation of SRO (001) planes can be parallel to the SrTiO₃ (001) surface. SRO/STO interface shows a slight lattice mismatch of 0.6% which is good for epitaxial film deposition. Investigation by STM and AFM surface topography of the SRO films showed a periodic step-terrace topography structure with an atomically flat surface, indicating step-flow growth mode.

Secondly, the PZT/SRO interface has shown an island growth mechanism. Crystal orientation is PZT [001] // SRO [001] and PZT [100] // SRO [100]. The AFM topography of PZT films shows a surface without terraces, but with a lightly sloping surface, indicating island growth. The lattice parameter of SRO is 2.7% smaller in the *a-b* plane and 5% smaller along the *c*-axis parallel to the film sequence, compared to PZT¹⁸. This relative high SRO/PZT lattice misfit prevents fully epitaxial growth and causes columnar structure in the PZT. The stress due to lattice misfit is relaxed at the column boundaries.

2.4 Etching

Photolithography was used to remove a small part of the PZT-film in order to be able to bond a wire to the bottom electrode. Photolithography is a process used in microfabrication to selectively remove parts of a thin film (or the bulk of a substrate). It uses light to transfer a geometric pattern from a photo mask to a light-sensitive chemical photoresist on the sample. A series of chemical treatments engrave the exposure pattern into the material underneath the photoresist. In our case the following procedure was used: spin the photoresist, heat up the sample to solidify the photoresist, illuminate the photoresist that needs to be removed, immerse the sample in photolithographic developer to lift-off the enlightened photoresist. Finally the sample is ready for chemical etching by PZT-etcher (10% HF, 10% HCl, 80% H₂O). This dissolves PZT, but preserves the underlying SrRuO₃ layer. Etching rate is approximately 14 nm per second, a layer of 400 nm needs to be immersed in the liquid PZT-etcher for 20 seconds.

2.5 Stencil deposition

Stencil deposition was used to create a finite sized top electrode on the sample of 1 mm². Pulsed Laser Deposition is able to deposit SrRuO₃ epitaxially on PZT, which operated as an electrode. By placing a mask in front of the plume, a direct copy of the structure of the mask can be made on the substrate. Advantage of small electrode in comparison to total coverage of SRO on the PZT is that electrical short through the PZT-layer is less likely to occur. Furthermore the magnitude of polarization current is linearly dependent on the area of the electrodes, so small electrode reduces charging effects emanating from this. The finite-sized top electrode is expected to introduce an asymmetry in the ferro- and piezoelectric behavior.

2.6 Characterization of structure and composition

Structural characterization of thin films was done by x-ray diffraction (XRD). The equipment that was used is a single-crystal diffractometer Enraf Nonius CAD 4 and the multi-purpose systems PANalytical X'pert MPD and a Bruker D8. The crystal orientations of the grown layers have been shown to agree expected crystal orientations, which were described above.

Surface topography of substrates and films were determined by the Veeco Digital Instruments Nanoscope Microscopy system. The system was operated in standard contact-mode or tapping-mode. In this way, the quality of the substrate and the deposited layers could be checked, for example, for contamination.

The ferroelectric properties of the sample were studied using an Aixact TF Analyzer 2000 FE-Module. This modular electrical characterization system consists of the Basic Unit to acquire and analyze data, a Probe Head consisting of the electrical hardware and a two probe head to Probe Stations connect to the sample.

2.7 Wire bonding

Platinum bond wires (with 2 % Cu added for flexibility) were used to connect to top or bottom electrodes to voltage source. Ultrasonic needle hammers the wire onto the surface, generating a contact area in the order of 100 μm in diameter. Resistance of the wires should be in the order of 5 Ω.

Oxidation of contact points can occur. Depending on the material, oxygen vacancies migrate, limiting conductivity near the contact point. Therefore it is necessary to check conductivity once a while. Furthermore the bonding process can damage the thin-film or even penetrate the film thus causing a short in the sample. This problem was avoided by gluing the bond wire to the sample, instead of hammering it ultrasonically. A small droplet of silver glue was placed on the top electrode using a brush. The minimum area covered by silver paint was found to be 200 μm. Subsequently the wire was carefully put into the droplet, followed by drying the silver glue.

Chapter 3 Piezo Force Microscopy

Piezoresponse Force Microscopy (PFM) or Piezo-Atomic Force Microscopy is a technique to image piezoelectric surfaces. The technique allows for piezoelectric amplitude and phase imaging with high resolution, down to 10 nm. It is relative insensitive to topography of the surface, due to lock-in amplification. Moreover the polarization of the film can be manipulated in case of ferroelectric materials by applying an electric field. A difficulty is that the contrast formation mechanism is still under debate in literature and can hardly be used for quantitative measurements. This is explained on basis of the not well-known electric field in the material and the complex tip-sample interactions. The aim was to explore possibilities of PFM, with special attention to the quantitative measurements of piezoelectric constant. This chapter will address the principle of operation, experimental conditions, results that were obtained.

3.1 Principle of operation

The Atomic Force Microscope (AFM) is an important tool at imaging, measuring and manipulating surfaces. AFM uses a micro-lithographically formed tip at the end of a cantilever (see Figure 3-1). An AFM senses the short range repulsive forces exerted by the sample on the tip. The deflection of the cantilever is measured using a laser beam reflected from the top of the cantilever onto a four quadrant photodiode. A feedback system adjusts the sample height by adjusting the Z-scanner to keeps the force constant. By scanning the tip over the surface, a topographic image of the surface is obtained.

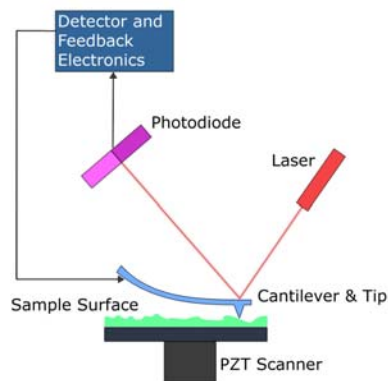


Figure 3-1 Schematic representation of the AFM system

PFM is a variation on AFM which is able to use the inverse piezoelectric effect to obtain local polarization patterns. While scanning a conducting AFM-tip in contact mode over the piezoelectric surface, a voltage is applied between the tip and bottom electrode. The generated electric field causes a piezoelectric deformation of the material underneath the tip, which is measured by the deflection of the cantilever. In PFM, the electric field is mainly applied in the out-of-plane direction and causes an in- and out-of-plane sample deformation. Usually the out-of-plane deformation is measured by the cantilever deflection, although it is also possible to use the lateral force imaging mode, to detect in-plane deformations by torsion of the cantilever. The amplitude of surface deformation depends on the piezoelectric coefficient, which is typically in the order of 50 pm/V for epitaxial PZT-based thin films, close to the morphotropic phase boundary. The longitudinal resolution depends on the detector, the lock-amplifier and feedback electronics. The lateral resolution conversely is defined by radius of the tip-surface contact.

Generally, PFM is used to image surfaces qualitatively, yielding spatially resolved information on domain size, domain stability or correlations between domain behavior and in inhomogeneities such as grain boundaries and switching behavior. However, attempts have been made in literature to quantify the results, meaning determining the magnitude of the piezoelectric constant. Paragraphs 3.3.3, 3.3.4 will study the important aspects in quantifying the piezoelectric response.

PFM measurements are based on the application of an AC signal and the measurement of the piezoelectric response of the material by the deflection of the tip. The input signal has the form $A_{in} \cdot \cos \varphi_{in}$, with A_{in} the amplitude in Volts and φ_{in} is the phase. Figure 3-2 shows the piezoresponse of two opposite polarized ferroelectric domains, which is $A_{out} \cos \varphi_{out}$. For a down-polarized domain, the deformation will be in-phase with the bias, an up-polarized domain will be out-of-phase relative to the bias. Lock-in detection is able to electronically enhance the signal and determine A_{out} and φ_{out} .

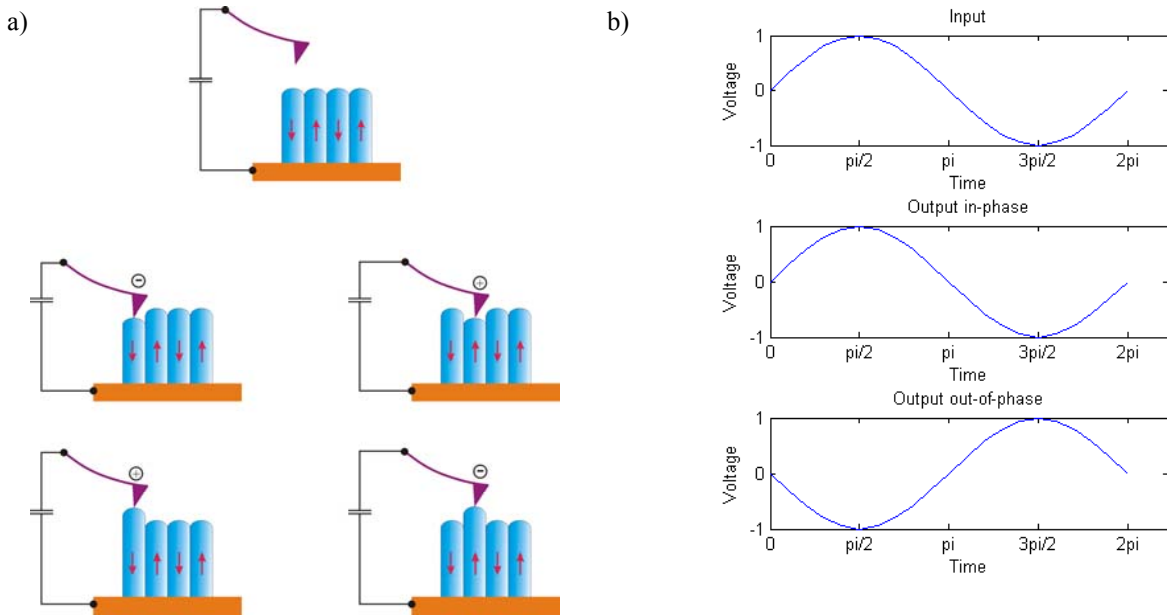


Figure 3-2 Principles of PFM a) On top no contact and resulting in no deformation and below an either a negative or positive biased tip in contact with an either up or down polarized domain and b) waveforms with $A \cos \varphi$ -form of the input, the output in-phase with input and the output out-of-phase in respect to the input

From figure 2-2 it can be seen that piezoresponse of a single up polarized domain is:

$$PR_{\uparrow} = A_{in} \cos \omega t \quad (3.1)$$

and of a single down polarized domain has an added phase shift π :

$$PR_{\downarrow} = A_{in} \cos(\omega t + \pi) \quad (3.2)$$

The real response originates from multiple domains, so instead of single values for the phase, either 0 or 180°, the phase can have intermediate values as well. Epitaxial films which have their tetragonal distortion out of plane can be modeled with only upward and downward domains. Figure 3-3 illustrates this for two domains.

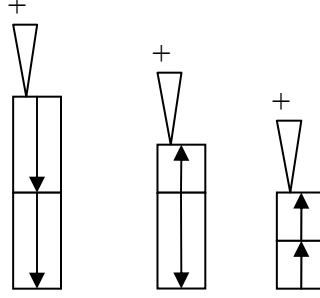


Figure 3-3 Model of the added piezoresponse (phase and amplitude) of two stacked domains

A simple model shows the total piezoresponse in phase and amplitude, given by the piezoresponse of N single domains

$$\sum_n PR_n = PR_{\uparrow} + PR_{\downarrow} = N_{\uparrow} A_{in} \cos \omega t + N_{\downarrow} A_{in} \cos(\omega t + \pi) \quad (3.3)$$

Where N_{\uparrow} is the number of upward polarized domains and N_{\downarrow} is the number of downward polarized domains. Using the Fourier coefficients a_n and b_n which are $a = A_{in} N_{\uparrow}$ and $b = A_{in} N_{\downarrow}$ this can be rewritten¹⁹

$$a \cos(\omega t) + b \sin(\omega t) = \sqrt{a^2 + b^2} \left[\frac{a}{\sqrt{a^2 + b^2}} \cos(\omega t) + \frac{b}{\sqrt{a^2 + b^2}} \sin(\omega t) \right] \quad (3.4)$$

Now include an angle φ ,

$$\sin \varphi = \frac{a}{\sqrt{a^2 + b^2}} \quad (3.5)$$

and

$$\cos \varphi = \frac{b}{\sqrt{a^2 + b^2}} \quad (3.6)$$

This is allowed since $\sin(\varphi)$ and $\cos(\varphi)$ are both ≤ 1 and $\sin^2(\varphi) + \cos^2(\varphi) = 1$. The result is

$$a \cos(\omega t) + b \sin(\omega t) = A [\sin \varphi \cos(\omega t) + \cos \varphi \sin(\omega t)] = A \sin(\omega t + \varphi) \quad (3.7)$$

With amplitude

$$A = \sqrt{a^2 + b^2} \quad (3.8)$$

and phase

$$\varphi = \arctan\left(\frac{a}{b}\right) \quad (3.9)$$

The resulting waveform is

$$f(t) = A_{out} \sin(\omega t + \varphi_{out}) \quad (3.10)$$

The ratio of up and down polarized domains will be reflected both in the amplitude and phase of the piezoresponse. The amplitude is:

$$A_{out} = A_{in} \sqrt{N_{\uparrow}^2 + N_{\downarrow}^2} = A_{in} \cdot N \sqrt{c^2 + (1-c)^2} \quad (3.11)$$

Where c is the ratio $\frac{N_{\uparrow}}{N_{\downarrow}}$ and N is the total number of domains, which is constant in this model. The phase is:

$$\varphi_{out} = \arctan\left(\frac{N_{\uparrow}}{N_{\downarrow}}\right) \quad (3.12)$$

The phase of measured signal is measured relatively to the phase of the applied ac-signal. It can be seen in equation 3.12 that the phase-shift is an indication of the number of domains that are polarized upward versus polarized downward. If all domains are polarized downward, the phase will be 0° and all domains are up the phase will be $+180^\circ$. Also can be seen that in this model the amplitude is not constant for all polarization states and will also depends on the ratio of up and down polarized domains. From this simple analysis, the amplitude depends on the polarization state and arrangement of the domains that are in the vicinity of the probe. It can be seen that the knowledge of the size and direction of the electric field is important for measurement of the piezoelectric constant.

Besides measuring the polarization of surfaces, the conducting tip can be used to influence polarization of the material, in case of a ferroelectric material. When the tip is biased above coercive field of the material, the spontaneous polarization will be reversed. Materials can be polarized up or down, which also is called 'writing'. A DC-voltage needs to be put to the tip, while the bottom electrode is grounded. This opens up possibilities for investigation of the stability of artificial polarized material, for example nucleation, lifetime or polarizability of domains.

3.2 Experimental

A Nanoscope IV Multimode microscope equipped with a PFM measurement option was used. Both controlling the microscope and acquisition and analysis of the data were done in Nanoscope software 5.12b. The tip and the sample can be biased (AC or DC) or grounded separately. A built-in lock-in amplifier acquires and modulates the data. The system can be equipped with the Signal Access Module (SAM), which can be used to access a variety of intermediate signals that are communicated between the controller and the Multimode.

Cantilever deflection Δz can be 0 – 400 nm, the spring constant k of the cantilever is 45 N/m, so forces F lie in the order of 1 μN . This force can be acquired by making a force calibration, linking the setpoint to the applied force. Assuming this force is distributed over a volume with dimension comparable to the tip-radius (± 20 nm), the pressure applied can be estimated.

$$P = \frac{F}{A} = \frac{1 \cdot 10^{-6} \text{ N}}{\pi(50 \cdot 10^{-9})^2} = 0.12 \cdot 10^9 \text{ Pa} = 120 \text{ MPa} \quad (3.14)$$

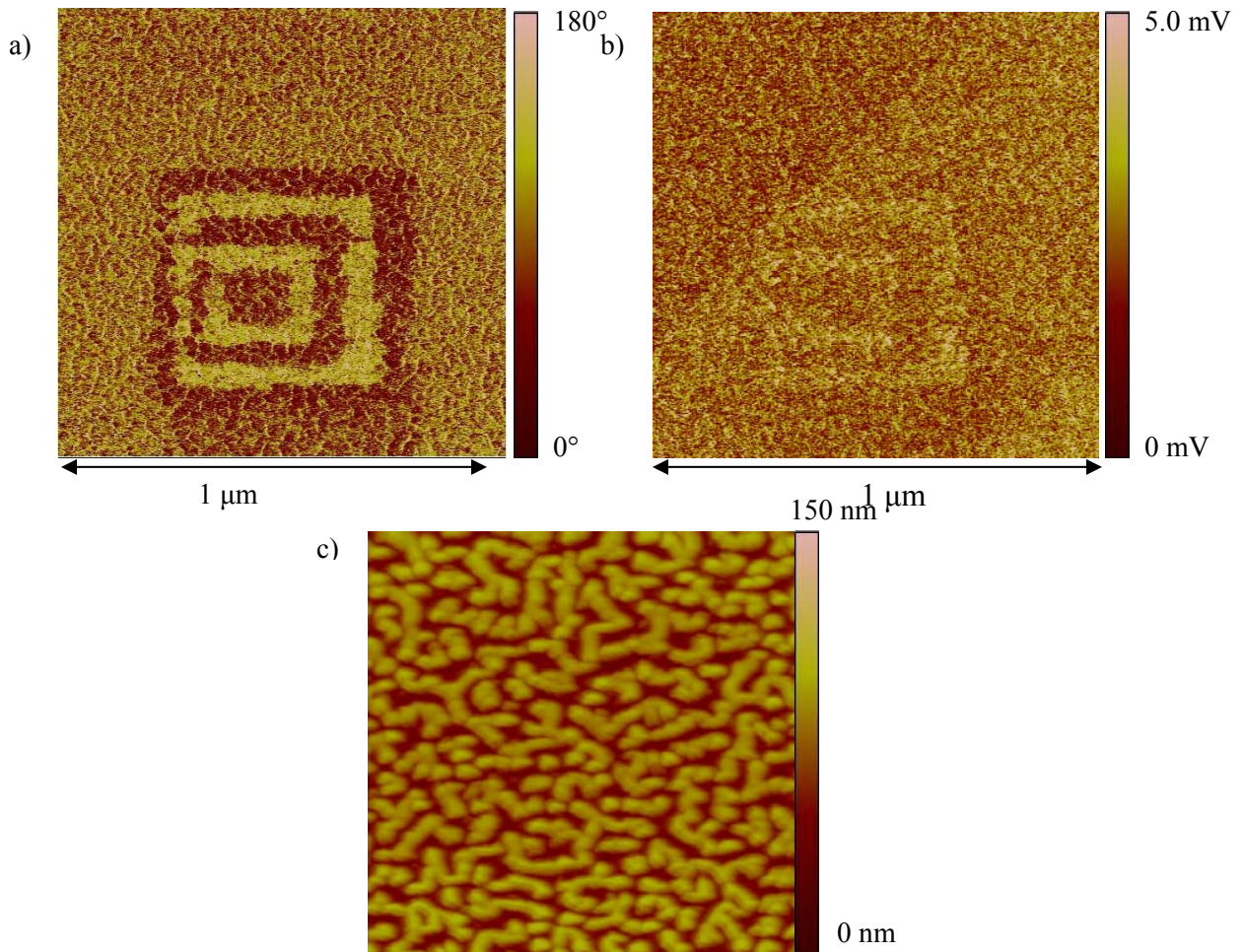
The pressure estimated here can influence the material properties. Stress and strain effects will be discussed in detail in paragraph 1.4.3. This shows that proper control of the setpoint deflection is important for good PFM-signals.

3.3 Results

This paragraph will describe the results obtained with PFM. Subsequently regular PFM, ferroelectric lithography and acquiring local hysteresis loops will be presented. Also a simple model of the electric field in PFM, tip-sample interactions and other issues concerning the tip will be described.

3.3.1 Regular PFM

The tip is scanned from left to right. Scan lines containing the amplitude and phase are generated and joined to form an image. A typical PFM-image is shown in Figure 3-5. The phase ranges from 0° to 180° and the amplitude is represented by a voltage. Figure 3-5c shows the topographic image of the PZT surface.



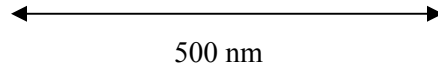


Figure 3-5 a) PFM-image showing the phase of the piezoresponse, several up and down polarized squares of decreasing size written over each other and b) the image of the amplitude of piezoresponse c) the topographic AFM image.

In the image several areas can be recognized. The outer areas were not polarized by an external applied field, showing a state of ‘natural polarization’. In the centre of the image, squares of +10 V and –10 V were written, of sizes 500 nm, 400 nm, 300 nm, 200 nm, 100 nm subsequently.

It can be noted, that a slight texture pattern can be observed in all areas of the image. This demonstrates that the polarization shows local variations. Furthermore, the square polarization patterns that were ‘written’, do not appear straight but have slightly frayed edges. An explanation for this can be that the polarization either follows the columnar structure of the PZT, or domains grow at a finite speed in outward radial direction around the contact area of the biased tip, in that way forming circular shapes.

It should be mentioned that it is possible that a ‘tip effect’ is occurring in the PFM images. Since the surface shows height differences and the tip has a finite size, the tip-sample contact may vary when scanning. To get an understanding of these effects, the PFM phase-image should be compared to the topographic image and the PFM amplitude-image.

Another effect that has to be kept in mind is the drift. The polarization of pattern was applied exactly in the middle of the scan. After finishing the writing, the same 1 μm area was imaged again. The pattern is shifted over 200 nm over 20 minutes, so the drift is estimated to be 10 nm per minute. This is remarkably high to be contributed to the piezo drift. It may be possible to reduce the drift significantly by using silver glue instead of sticky tape to mount the sample on the sample holder.

3.3.2 Ferroelectric lithography

The PFM setup offers the possibility to control the tip as a nanoscale movable electrode on the surface. This allows for local modifications in polarization. When applying the biased tip to ferroelectric films, the polarization can be switched locally. This technique can be called ferroelectric lithography. It can enable useful measurements on polarization dynamics of ferroelectric films, such as growth and stability of domains. In this paragraph a pattern will be polarized onto a PZT surface, to demonstrate ferroelectric lithography.

The Nanoscope software uses a script to position and move the tip over the surface, called the ‘nanolithography’ option. A sequence of commands can be executed by the microscope to control the position, tip voltage, deflection setpoint or to engage and retract the tip to the surface. It can be seen that nanolithography option also can be used to, for example, scratch the surface, by applying high force to the tip. Ferroelectric lithography is categorized as part of scanning probe lithography.

Although fully integrated plug-ins for the nanolithography on SPM systems exists, it was not available on the system used here. Therefore a program C++-builder was used to generate a dynamic library link-file (extension .dll), which can execute the same functions. This file should contain the pre-specified functions and accessory parameters. The Nanoscope software then can run this file and will then execute the commands in a chronological order.

Using this method, a pattern consisting of the ‘IMS’ characters, was polarized on the PZT sample. Immediately after running the script, the surface was imaged by PFM, using the same tip. The characters appeared in the image, see

Figure 3-6

a)

180° b)

5.0 mV

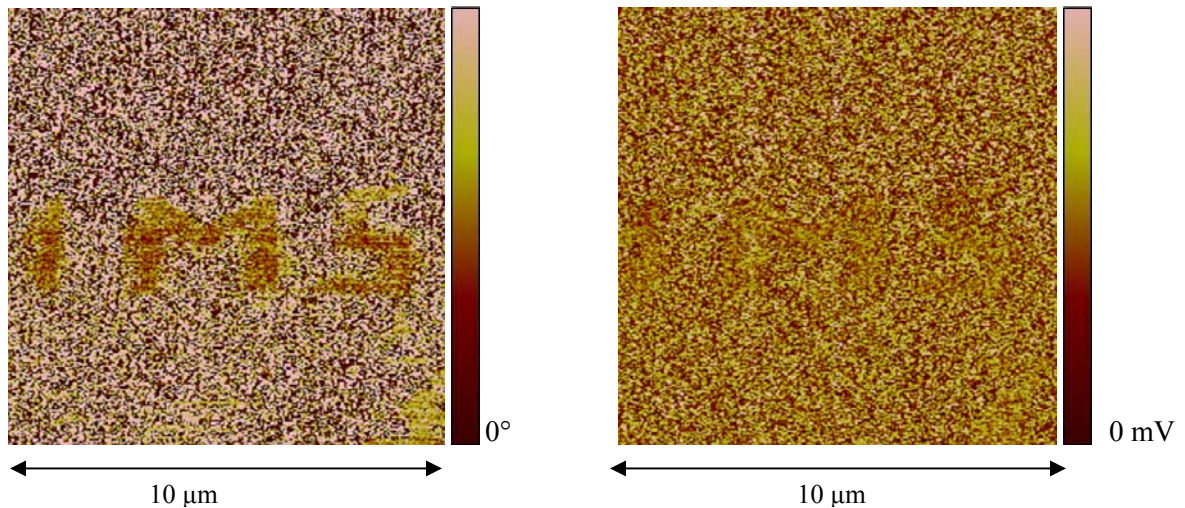


Figure 3-6 PFM-image of PZT polarized with a pattern of characters 'IMS' a) phase b) amplitude.

Using the nanolithography-option, it is possible to demonstrate the suitability of ferroelectric materials like PZT for non-volatile memory applications. By applying short voltage pulses in a fixed pattern, it is possible to polarize small areas on the surface. Subsequently the polarization can be read out by standard PFM, see Figure 3-7. The high storage density of PZT obtained is 4 Gb/cm^2 , which is higher than any current application or developing technique is capable of²⁰.

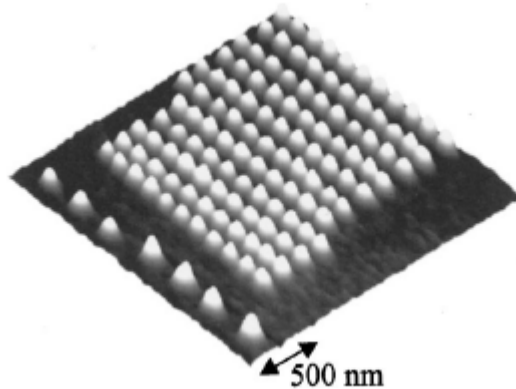


Figure 3-7 Piezoelectric image of an 11x11 array, written at 4 Gb/cm^2 with 10V pulses of 3 ms.

It can be seen that using the local polarization by an external field, measurements can be done of polarization and domain dynamics on surfaces. For example, the stability of domains for different materials properties, the speed of domain growth can be determined²¹.

3.3.3 Local quantitative measurements by PFM

The usual PFM measurements are capable of imaging ferroelectric domains, using the PFM phase information. However, also efforts have been made to determine the piezoelectric constant, using the PFM amplitude. This paragraph will describe how this can be done, and the disadvantages that are associated with this.

Two approaches have been used for this²²:

- Sweeping the amplitude of the testing AC-voltage from zero up to the local coercive voltage of the sample. The piezoelectric constant can be easily calculated from the slope of the linear dependence. In case of ferroelectrics as soon as the AC amplitude is higher than the local coercive voltage, the polarization starts to switch with the same frequency as the AC voltage, leading to a decrease of the response.
- Sweeping a DC bias source connected in series with the AC-voltage source. Local hysteresis loops can be constructed from the AC-signal response. From these hysteresis loops the local coercive field and piezoelectric constant can be determined.

However, some drawbacks from these measurements have to be recognized. First, due to the small size of the tip, the electric field is highly non-linear. The polarization is distributed unequally throughout the film, which means the electric field is not known and the PFM-images, piezoelectric constant and hysteresis loops cannot be calculated accurately. A model to calculate this non-linear field inside the film is presented in the next paragraph, 3.3.4.

Secondly, difficulties related to positioning the tip at a specific location on the surface (due to drift), as well as long acquisition times, limit these studies to only a few points on the sample surface thus hampering correlation between the material's microstructure.

3.3.4 Modeling of the electric field

The quantitative PFM-measurements, mentioned in previous paragraph 3.3.3, make use of a conducting tip with a radius in the order of 20 nm. The dimensions of the tip do not obey the criterion for the ideal capacitor approximations ($A \gg d$), which was described in paragraph 1.3.1. Therefore the electric field which is generated inside the material is highly non-linear. A model is constructed to calculate the electric field inside the material and interpret the validity of quantification of PFM measurements, see Figure 3-8.²³

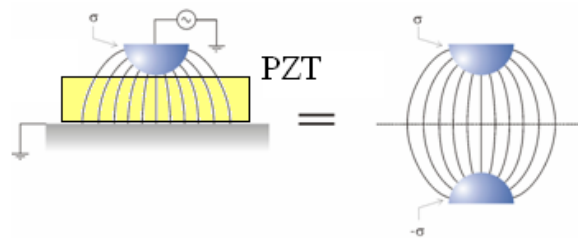


Figure 3-8 Model of the electric field inside the material. Electric field lines are curved indicating the strength of the electric field is rapidly decaying with increasing distance from the tip

The potential for a tip with a finite radius R , film thickness d and z position above the substrate, using the method of mirror-charges.

$$V_{tot}(z) = \frac{R\sigma}{2\epsilon_0} \left(\frac{1}{(d-z)} \left(\sqrt{R^2 + (d-z)^2} - \sqrt{(R-(d-z))^2} \right) - \frac{1}{(d+z)} \left(\sqrt{R^2 + (d+z)^2} - \sqrt{(R-(d+z))^2} \right) \right)$$

The field is the derivative of the potential. The dielectric constant of the thin film is neglected, to simplify the model. As can be seen in Figure 3-9, for a 50 nm film the electric field is concentrated in the first 10 nm under the tip. In the remaining 40 nm, the field strength is below 10 %.

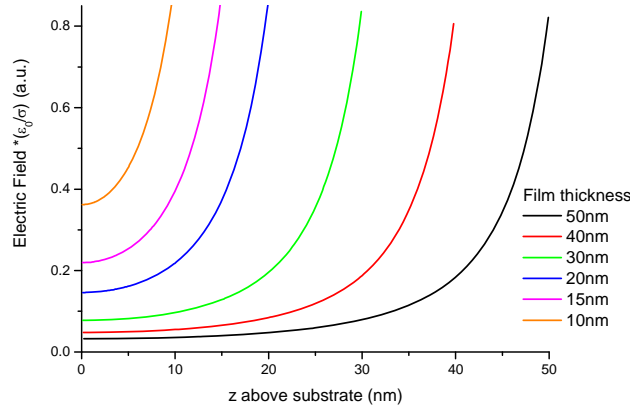


Figure 3-9 Electric field strength as a function of height above the substrate, for changing thicknesses of films.

The model shows that the electric field varies heavily throughout the film. The variation limits the use of PFM for the quantification of the piezoelectric coefficient. Several efforts in literature have been made to model the electric field and claim to have determined the field, but most authors mention large error-bars in their results.

The model does not incorporate the dielectric constant of the material. Since this constant can be very high for titanate based ceramics (see paragraph 1.1), and for PZT is in the order of 1000, it can be important to think about the consequences. In case the permittivity of the material increases bigger than 1, the ratio of charge and distance of the tip and the induced mirror charges in the surface changes. Still, Harnagea showed by a similar model, where the ratio of permittivity determined the ratio of magnitude of the mirror charges, a voltage drop over the first 30% of thickness of the dielectric is almost 90% of the voltage applied to the tip.⁷ Conclusion of these calculations is that PFM can only probe a volume very close to the tip and no exact knowledge of the electric field can be obtained, which is necessary for quantitative measurements of the piezoelectric coefficient.

3.3.5 Cantilever-sample interaction

The PFM technique is based on the interaction between the tip and sample. Since many mechanisms have to be included, this interaction is very complex. This paragraph will give a short overview of the most important interactions and the consequences for choice of tip force constant for PFM.

The most important forces in PFM can be recognized are:

- Local electrostatic
- Non-local electrostatic
- Electromechanical

Electrostatic interactions are a result of interactions between localized space charges and the applied voltage to the tip. These localized charges are dominated by bound charges determined by the polarization of the domain that are close to the tip. To estimate the influence of the electrostatic contribution, it should be compared to the tip indentation force. The indentation force is $F_{ind} = k \cdot d$ (equation 3.15), where k is the force constant of the cantilever and d deflection resulting from the setpoint and the electrostatic force is $F_{el} = C(V_{tip} - V_{surf})^2$, where C is the tip-surface capacitive gradient and V is the potential of respectively the tip and the surface. For standard PFM operation, F_{el} can be estimated to be 10 nN and the F_{ind} to be in the range of 1 nN to 10 μ N. For normal operation a force constant $k > 10$ N/m and a minimum cantilever

deflection of only 10 nm are reasonable. The resulting force will be 100 nN and already be significant higher than the electrostatic force F_{el} .

The second factor is the non-local capacitive electrostatic force existing between the cantilever and sample. These non-local electrostatic contributions are empirically found to be negligible for force constants higher than 1 N/m.

Finally, electromechanical interactions are the mechanical deformations induced by electrical voltage to the tip. This is the interaction that is detected for PFM. A good electromechanical contact is important to obtain reliable PFM data and therefore the contact mechanisms for electromechanical interactions are studied with care. The interaction involves two aspects: the transmittance of the tip potential to the sample, and the transmittance of the bias-induced sample deformation back to the tip.

Considering the first aspect, a dielectric tip-surface gap can significantly attenuate the surface potential. This gap can originate both from intrinsic properties of the dielectric tip-surface junction and due to the presence of 'dead layers'. The force constant of the tip and the setpoint deflection of the feedback system are determine the indentation force (see equation 3.15), and are important for determining the contact quality.

Three indentation regimes can be defined²⁴, see also Figure 3-10.

- Strong indentation, $V = V_{tip}$
- Limited contact indentation, $V = \gamma V_{tip}$, γ is an attenuation factor.
- Weak indentation, no effective contact

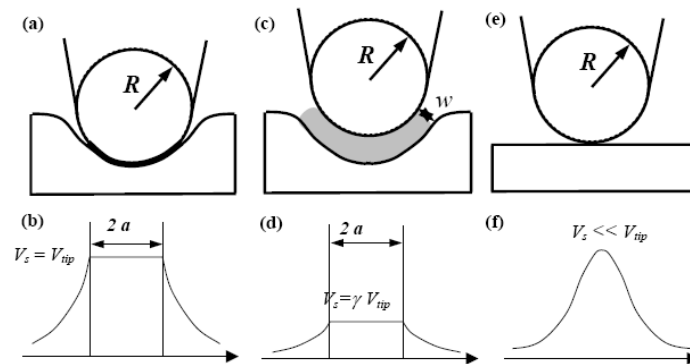


Figure 3-10 Indentation regimes for a spherical tip indenting the surface. Geometry and surface potential for a,b) Strong indentation, c,d) limited contact indentation e,f) weak indentation

Indentation regimes depend on several parameters, such as indentation force, which is controlled by the setpoint deflection, tip diameters and applied voltage. Contrast maps have been calculated by Kalinin and Bonnell²⁵, for parameters tip radius and indentation force and are shown in Figure 3-11.

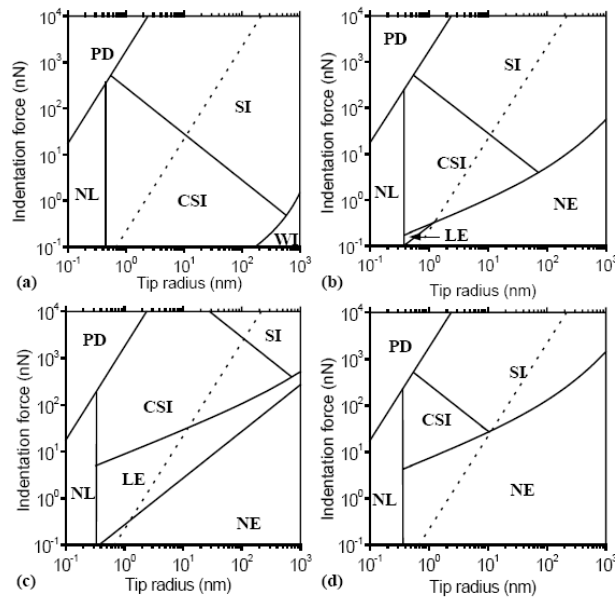


Figure 3-11 Contrast Mechanism Maps of piezoresponse force microscopy. SI is strong indentation regime, CSI - contact limited strong indentation, WI - weak indentation regime, LE - linear electrostatic regime, NE - nonlinear electrostatic regime, NL - non-local interactions, PD - plastic deformation. The dotted line delineates the region where stress-induced switching is possible. (a) $w = 0.1 \text{ nm}$, $\Delta V = V_{\text{tip}} - V_s = 0 \text{ V}$, (b) $w = 0.1 \text{ nm}$, $\Delta V = 1 \text{ V}$, (c) $w = 1 \text{ nm}$, $\Delta V = 1 \text{ V}$, (d) $w = 0.1 \text{ nm}$, $\Delta V = 5 \text{ V}$.²⁴

From these contrast mechanism maps it can be seen that indentation force should be high enough to ensure strong indentation. In practice the deflection setpoint and force constant of the cantilever need to be tuned (see also equation 3.1). A general assumption is that for a force constant of 42 N/m the electrostatic forces can be neglected. These indentation regimes are widely accepted and applied in PFM-community. Results in paragraph 3.3.6 match the argument shown above.

Also possible stress-induced polarization switching by indentation force is shown by the dotted line in these graphs. The huge pressure that is applied by the tip may also decrease the piezoresponse. For example Zavala et al. reported a 30% decrease of the piezoelectric constant of undoped PZT while increasing the contact force from 10 μN to 23 μN .²⁶

3.3.6 Probes and degradation of the sample

The probe is by far the most important part of the PFM system. The high resolution of AFM and PFM depends on the dimensions of the tip. However it is extremely sensitive to processes at the tip-sample interface. In the case of PFM, the tip should have both good mechanical and electrical contact. The effects that influence this contact will be investigated in this paragraph.

The tip has a pyramid shape and is mounted on a cantilever, see Figure 3-12. Two types of tips were used. Antimony doped (n) tips (TESP) with force constant 42 N/m and Silicon ElectriMulti75 (3 N/m), which is coated with Platinum Chrome on both sides. Typical height of the tips is 20 μm .

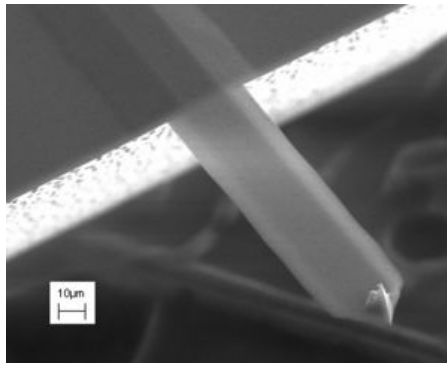


Figure 3-12 Image typical AFM- tip

Besides being the most important part, the tip is also the most vulnerable part of the PFM system. Several processes occur when the tip is brought in contact with the sample. In practice the tip and the sample will degrade by several factors

- Mechanical forces
- Conductive heating leading to burning
- Collection of dust, dirt and moisture
- Electrochemical reactions at the tip-surface junction

It is possible that mechanical forces exerted on the tip are very large (see equation 3.14) and cause metal peel-off or tip shape changes. It can lead to a considerable increase in tip radius which implies loss of spatial resolution. An increase in tip radius can force the tip-sample interaction out of the strong indentation regime, decreasing the electromechanical contact. Furthermore electrical conductivity may be lost by damage of the conductive layer in case of coated tips.

This observation leads to the following practical consequences. A tip needs to be replaced often, depending on the results obtained, possibly every day. Forces were estimated to be between 10 nN and $10\text{ }\mu\text{N}$. High forces applied to the tip should be avoided. The scanning speed in PFM measurements is typically $>10\text{ nm/s}$. High scanning speed should be avoided, since rough and dirty surfaces can degrade the tip.

SEM images of a new and a used tip were made, as shown in Figure 3-13. The loss of tip sharpness is clearly visible. Only a few scans with a tip can degrade the tip from its radius of 20 nm to $50\text{-}100\text{ nm}$ ²².

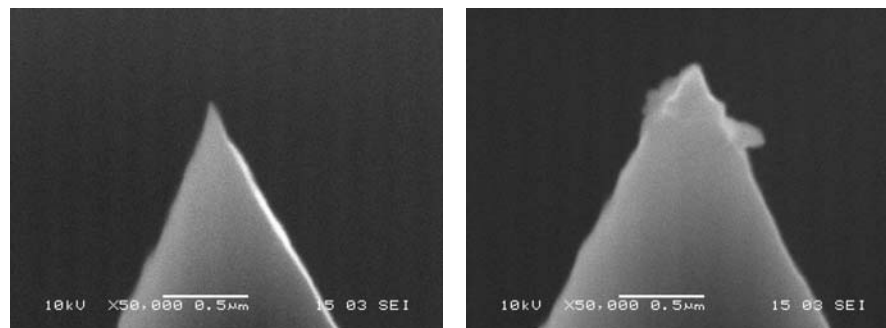


Figure 3-13 Scanning Electron Microscope images of PFM-tips a) new tip b) used tip, approximately 1 hour continuous scanning

Resistive heating due to the induced current may lead to burning of the tip. Especially tips that are coated with a thin conductive layer may be vulnerable to high current. High voltages have shown a sudden disappearance of the signal, probably due to tip burning and should be avoided.

The formation of a dead layer can be caused by a chemical reaction for example oxidation or the deposition of a layer of dust and moisture. This results in a degrading contact between the tip and the sample. In practice, samples age very rapidly. Samples of a few weeks old have shown little or even no piezoresponse

at all. Furthermore the tip may collect dust or dirt lying on the surface, which might lead to a large contact area. Also a water layer increases both the mechanical contact area and electrical contact area. Figure 3-14 shows a SEM image of a tip that was used extensively. Figure 3-14b shows a PFM image that was made by this tip, showing a very poor lateral resolution. First a square was tried to polarize and subsequently the PFM image was measured.

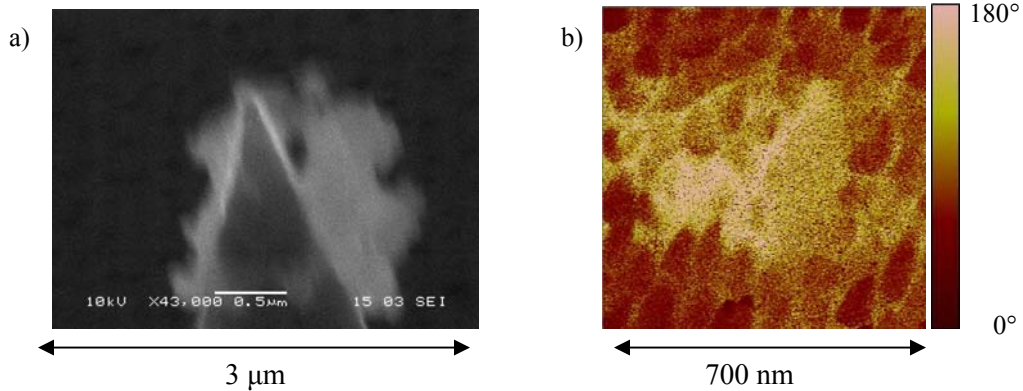


Figure 3-14 a) Scanning Electron Microscope image of a tip that was used 2 weeks and b) resulting PFM-image

Table 3-2 gives an overview of the operation of the two types of tips that were used. For writing a very good electrical contact is needed. Therefore the high force constant tip (TESP) shows advantages here. Sensitivity is better for a tip with a low force constant, provided the electrical contact okay. Also electrostatic interaction might start to play a role for a low force constant. A high current will burn the ElectriMulti75 tip, since this one is coated by a thin layer of Cr/Pt. The doped TESP tip is fully conductive and can handle high currents better, although leaky samples might still result in tip damage.

Table 3-2 An overview of the tips that were used and their properties

	TESP	ElectriMulti75
Writing	Easy (high force)	Difficult (low force)
Sensitivity	Good	Better
Allowable voltage	No limit	<6-8V (burning)

Chapter 4 Piezoresponse Scanning Tunneling Microscopy (PSTM)

Piezoresponse Scanning Tunneling Microscopy (PSTM) is a new technique to accurately measure the displacement and hysteresis loops of piezoelectric thin-films. A top electrode was added to the sample configuration to induce a uniform electric field in the sample and a Scanning Tunneling Microscope was used to measure the displacement of the surface. With this technique lateral resolution is lost but the electric field is well defined for analysis of the piezoelectric coefficient d_{33} . This chapter will describe the basic principles of PSTM, discuss the experimental issues and present the results that were obtained.

4.1 Sample configuration

The sample configuration for PSTM is changed with respect to the configuration used in PFM. A major concern in quantitative piezoresponse measurements is the non-uniform electric field that is applied in the material (see paragraph 3.3.4). In order to obtain a uniform electric field inside the material, a conducting top electrode was added to the sample configuration. A layer of SrRuO₃ of thickness of 50 nm was deposited through a stencil on top of the PZT. The analysis of this configuration by PSTM has not been reported before, only an NSTO-PZT (80/20)-Au or polymer samples have been investigated. For detailed description see paragraph 2.3. Since $A \gg d$, the sample behaves like an ideal capacitor. The electric field is defined by the voltage V applied over the capacitor plates and thickness of the layer d :

$$E = \frac{V}{d} \quad (4.1)$$

Figure 4-1 shows the configuration:

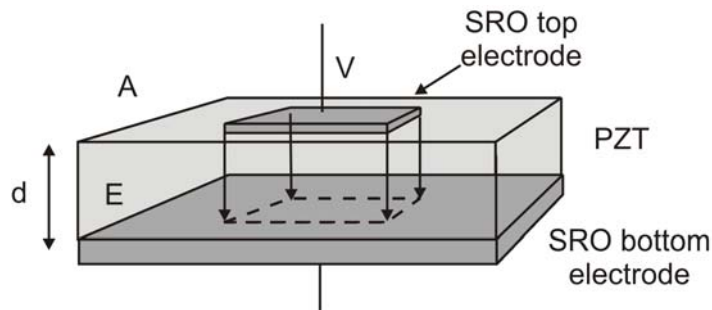


Figure 4-1 Sample configuration for PSTM measurements

The piezoelectric sample deformation will be perpendicular to the top electrode and shows a linear behavior as a function of the voltage, with piezoelectric coefficient d_{33} .

$$\Delta z = d_{33} \cdot V \quad (4.2)$$

The deposition of the conducting top electrode makes it possible to use Scanning Tunneling Microscopy as the deformation measurement technique. Since a voltage should be applied between the top and bottom electrode, the piezoelectric material between the electrodes cannot be 'leaky' and shortcuts should be avoided. This SPM technique can only be operated on conducting surfaces, and is expected to have a higher longitudinal resolution compared to AFM.

4.2 Scanning Tunneling Microscopy

The principle of a Scanning Tunneling Microscope (STM) consists of scanning a tip over a conducting surface at a constant tunneling current. A feedback loop adjusts the tip-sample distance until a current setpoint value is reached. In this way a surface topography can be constructed. The reason for the

outstanding z-resolution is that the tunneling current shows an exponential relation to the tip-sample distance²⁷.

$$I_{tun} \sim e^{-(2/\hbar)\sqrt{2m\phi}\cdot d} \quad (4.3)$$

With m being the electronic mass and ϕ the effective work function of the imaged material, which for our experimental condition for SRO is in the range of 100 meV.²⁸ With a barrier height of a few electron volts, a change of the tunnel barrier width by a single atomic step ($\sim 2\text{-}5 \text{ \AA}$) changes the tunnel current up to three orders of magnitude. Generally the tip-sample distance is roughly 1 nanometer. Figure 4-2 shows the tunneling current between tip and sample.

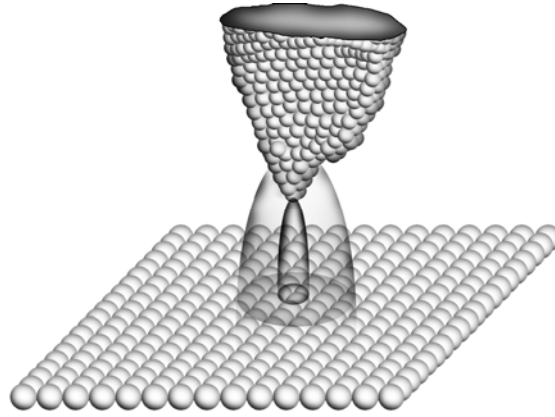


Figure 4-2 Tunneling between tip and sample. Electron flow varies exponentially with tip sample distance²⁹

The Scanning Probe Microscopy was used to study and control the ferroelectric material was first done in 1991, when Birk et al.²⁸ measured the piezoelectric constant of a ferroelectric polymer. Soon people switched to contact-AFM with a conducting tip, tempted by the promise of localized analysis. STM was not reported anymore, until Kuffer³⁰ et al. used it to study measure piezoelectric response of $\text{Pb}(\text{Zr}_{0.2}\text{Ti}_{0.8})\text{O}_3$.

4.3 Principle of operation

By locating the STM-tip above the top electrode, the out-of-plane deformation will be measured as a function of applied voltage. The voltage is applied directly via a wire bond to the bottom-electrode. A triangular voltage is applied over the capacitor plates. The expected piezoelectric behavior of a ferroelectric material is shown in Figure 4-3. At voltages higher than the coercive voltage, a frequency doubling occurs, due to ferroelectric switching of the polarization.

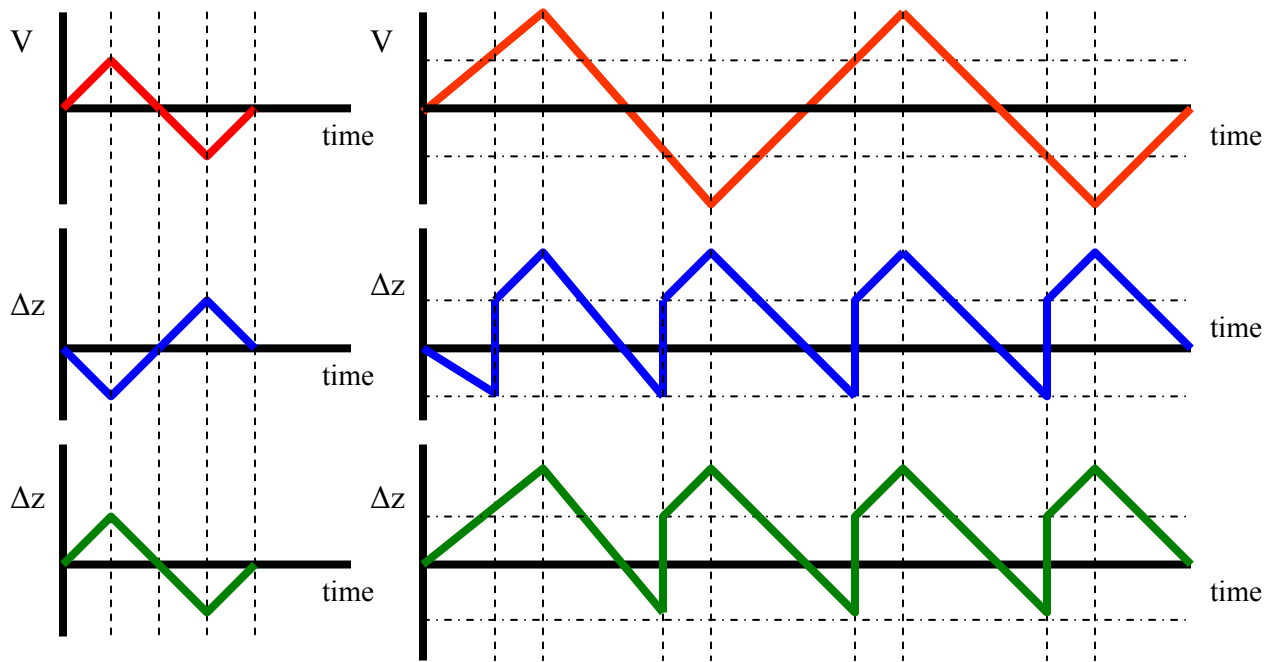


Figure 4-3 Piezoresponse in ferroelectrics: Applied voltage V (top) and piezoresponse Δz under coercive voltage (left) and above coercive voltage (right). Initial polarization upward (middle) generates an initial out-of-phase response and initial polarization downward (bottom) generates an initial in-phase response. After that, the piezoresponse above coercive field is independent of initial polarization.

It can be seen in Figure 4-3 that the initial polarity of the material determines the shape of the piezoresponse, only for a bias under the coercive voltage. For bias under the coercive voltage, a downward polarized sample will respond out-of-phase, an upward polarized sample will respond in-phase. In case of a bias above the coercive voltage, the response is independent of the initial polarization. Only the first cycle depends on the initial state, after that the piezoresponse will come to its steady shape. In theory, this shape is always the same and can not be mirrored around the horizontal axis. From these graphs the deformation as a function of applied field or voltage can be constructed, also called the d-E loop or ‘butterfly’ loop, Figure 4-4.

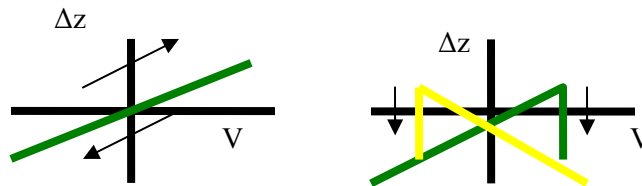


Figure 4-4 Schematic piezoelectric deformation as a function of voltage for voltages a) below the coercive voltage and b) above coercive voltage

The piezoelectric coefficient can be determined by slope of the butterfly loop, $\frac{d(\Delta z)}{dV}$. The gradient of the d-E loop generates the piezoelectric coefficient, illustrated by Figure 4-5. A striking feature is that the ideal piezoresponse in Figure 4-5b shows two spikes of d_{33} , since exactly at the switching voltage the gradient of the d-E loop is infinite.

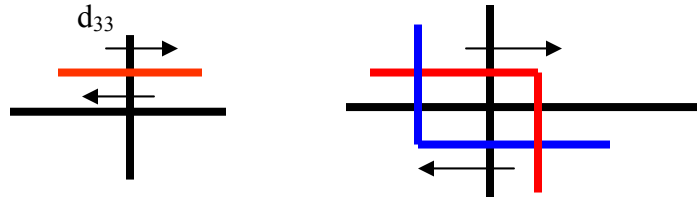


Figure 4-5 Schematic d-E loop for a) bias below coercive field and b) above coercive field

4.4 Experimental

The setup can be split in three main components:

- Microscope
- Computer & Electronics
- External Equipment

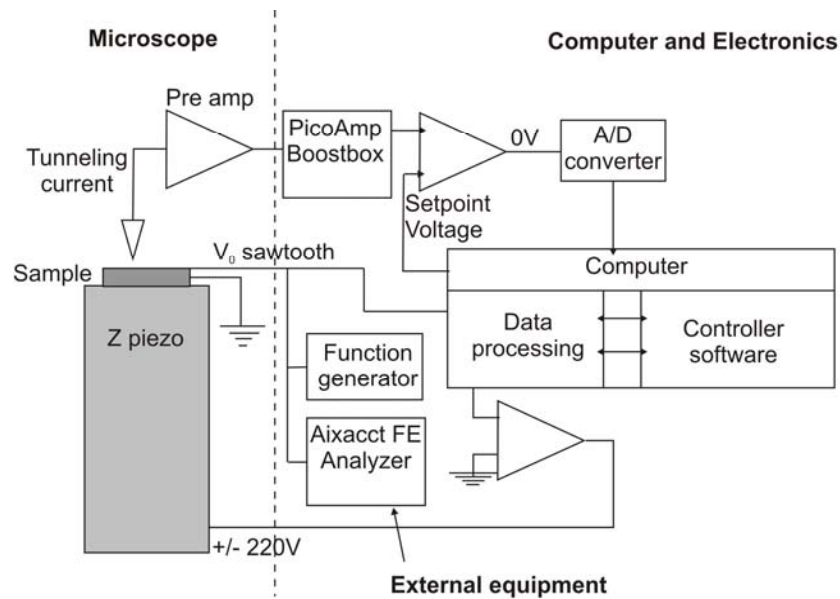


Figure 4-6 Schematic setup of the PSTM system.

The microscope is a Multimode STM with a special low-current amplifier, which measures current in the picoAmpere range (Model MMSTMLC). This STM is useful for high-sensitivity and small height changes. A low-current amplifier ('PicoAmp Boost Box') was placed between the Nanoscope IV controller and Multimode STM. Since the current limit of this microscope is 2nA, the setpoint current was set below this value, typically 200 pA. The default Z-sensitivity calibration value was adjusted to the Boost Box-gain that was used. This value automatically alters the overall calibration file that the software uses, and it is independent of the AFM measurements done on the system. The software used for PSTM was Nanoscope version 6.13r1.

The bias and setpoint current should be set according to the conductivity of the sample under investigation. Samples which are excellent conductors (e.g., gold) can operate with a bias of 1 to 50 mV. Conversely, if the sample is a semiconductor, the bias may have to be set higher (e.g., 100 mV) to obtain an image. For regular STM, the current can be set from 0.2 to 10 nA. In our case, currents above 200 pA and bias 200 mV generated satisfying results for SRO.

Platinum-Iridium tips are made by 0.25 mm wire cut under $\sim 60^\circ$. This material has the advantage that it does not oxidize, contrary to Tungsten tips. Pt-Ir softness allows the tip to be cut easily, contrary to Tungsten which needs an etching process to create a sharp tip. Not all installed tips prove to be work properly in the STM; the atomic arrangement at the sharpest part of the tip may deviate from the ideal form, an atomically sharp tip. Because the tip is not in contact with the surface, no degradation of the tip will occur that is due to tip-sample interaction, as opposed to (contact) AFM. However the tip is in the order of nanometers separated from the surface, a tip-crash can happen easily.³¹

A special sample holder was constructed to allow easy mounting of the sample into the STM-head. The voltage is applied externally via connecting wires, which are soldered to the copper plates. These wires are flexible to minimize vibrations passed on to the sample holder, minimize possible movements due to weight of the wires. The wires are shielded to minimize electromagnetic noise picked up by the wires. The sample holder is magnetically connected to the top of the piezo tube. The sample is mounted on the sample holder by silver glue, which has to dry for several of minutes to avoid unwanted movements of the sample. Figure 4-7 shows the sample holder including an installed sample.

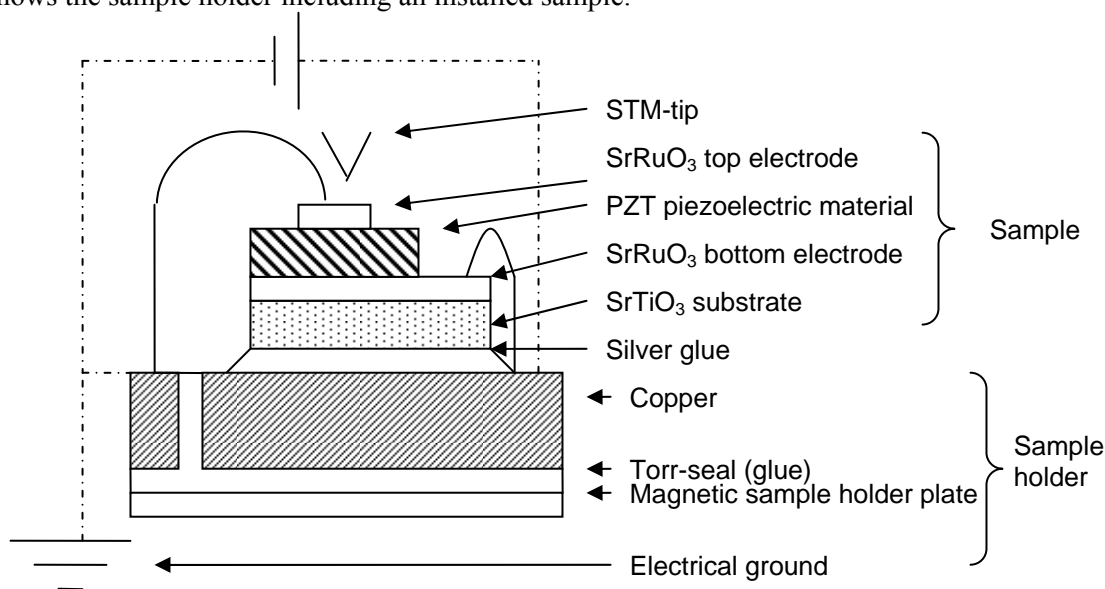


Figure 4-7 Sample configuration for PSTM

The top electrode was deposited by stencil deposition. It has a size of 1 mm^2 , so that a bonding wire can be glued to it easily and leaves space to engage the STM-tip to it. The glue can be placed partially off the top electrode, as long as contact is maintained. A STM image from the top electrode of the sample is shown in Figure 4-8.

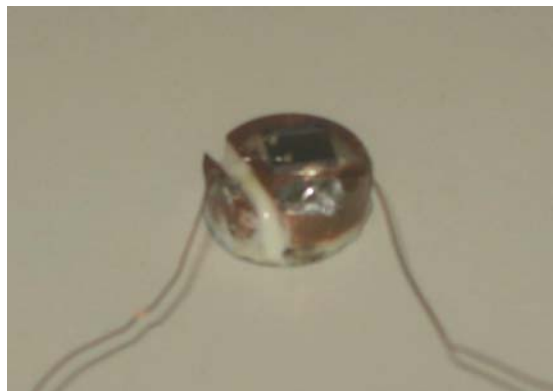


Figure 4-8 Photo of sample holder and sample

Prior to the measurement, the following preparations were performed. First the tip was engaged onto the SRO top electrode, and a STM-image will be generated. Subsequently the tip is maneuvered to a smooth terrace. This is done to avoid any influence of the surface topography on the intended STM measurements. The scan size is set to zero, which results in an effective scan size of 1x1 pm. This is the minimum possible scan size that the controller can set. Still, the microscope is in scanning mode, which means scan lines are displayed in image. The scanning rate can be chosen for normal STM-operation between 0.1 Hz and 10 Hz.

For a STM under ambient conditions, the sensitivity is mostly limited by noise. Physical noise filtering is applied in three ways. One is the placing the STM-unit onto a granite block. Secondly the whole is suspended by cables of 1.5 m, holding the granite block and STM. Finally, a grounded metal bucket was placed over the STM-unit, to shield the microscope from electromagnetic noise. Electronic noise filtering is done by the PicoAmpBox, which amplifies the signal in a bandwidth that can be chosen manually.

The STM uses a feedback system to maintain a constant tip-sample distance. The parameters for the feedback system were tuned to obtain a good image. Since the piezoelectric displacement measured by the STM is a triangular waveform with a constant positive or negative slope, the proportional gain will not be sufficient to effectively eliminate the error signal. This means the integral gain is most important to obtain good quality images. In practice a constant current mode can be set by and the integral which was < 1.0 and the proportional gain that is < 0.5 . For the constant current mode the integral gain was > 1.0 and the proportional gain is > 0.5 .

Another feature of the STM which is important for good results is the A-D conversion. The current and the height will be converted to a digital signal. The Z-range is an important parameter in this matter. It determines the resolution of the A/D conversion. In the case of small deformations and large z-scale, the data cannot be converted properly. The Z-range was lowered from the maximum 3.7 μm to 1-2 μm (for the E-scanner). In case of an increase of the amplitude of the piezoelectric deformations or misalignment of the tip, the Z-range was increased to avoid it from going out-of-range. In that case the piezo will loose contact or crash into the surface.

External equipment is:

- FE-tester Aixacct, used for data acquisition and can also be used to generate a voltage of any waveform. This apparatus is designed to do measure dE-loops. It generates a waveform and simultaneously captures the displacement data. This displacement is represented by a voltage coming from the Signal Access Module, for example the voltage on the z-piezo, which follows the surface when the STM is in feedback-mode. A proper calibration should be done to determine the voltage to displacement constant.
- Function generator, Hewlett-Packard, used to generate a voltage of any waveform on the sample. To obtain PSTM pictures with piezoelectric deformation occurring perpendicular to the scan-lines, the frequency was determined up to 4 decimals exactly.

4.5 Results

This paragraph will give the results that were obtained on the fabricated sample. Subsequently regular STM measurements, macroscopic polarization measurements, the PSTM measurements, an exploration of spectroscopic STM measurements and a short study of charging and electromagnetic effects for this system will be presented.

4.5.1 Topography STM

A typical STM-topography of terrace-structures of SRO is shown in Figure 4-9a. Hairlines can be seen in the image Figure 4-9b, which are likely to be discontinuities in the crystal growth and are induced by terrace steps of the STO substrate.

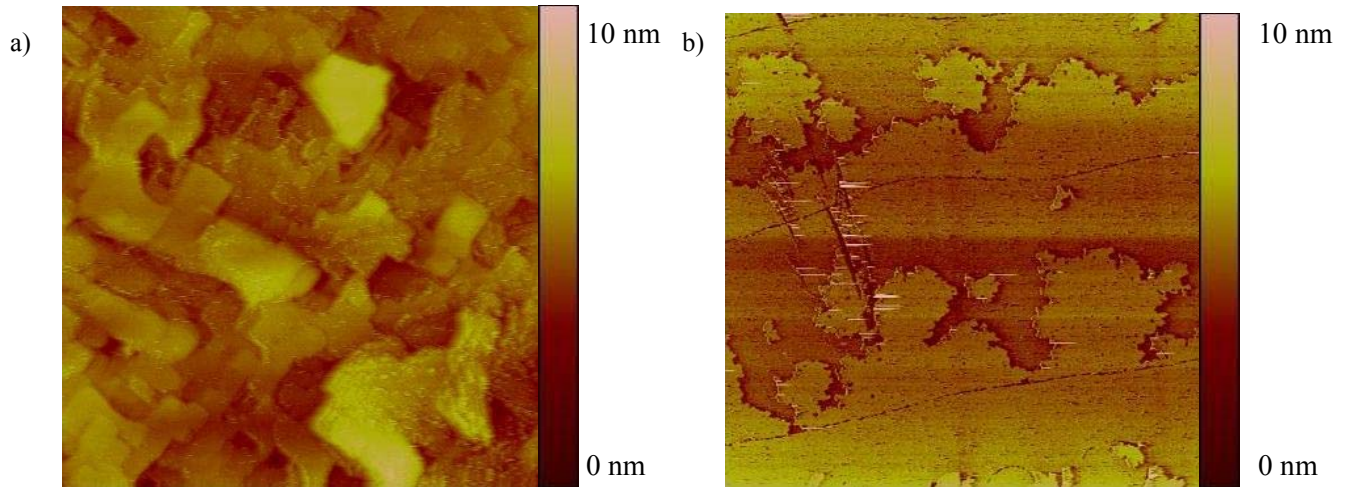


Figure 4-9 STM-images of a) Topography of SRO top electrode deposited on PZT and b) 4 monolayers SRO on STO-substrate

4.5.2 Macroscopic polarization measurements

A macroscopic direct measurement of polarization was done on the PSTM sample, as described in paragraph 4.1. The Aixact Analyzer 2000 FE-Module was used. The probes were placed on the bottom and top electrode, to measure the current while a voltage is applied. Coercive field appears to be between 3 and 4 V. The remnant polarization is $43 \mu\text{C}/\text{cm}^2$. Electric breakdown occurs when the sample is biased above ~ 8 V for a 100 nm thick film. The loop is slightly asymmetric. This may be caused by electrode effects, for instance differences of the interface between PZT and SRO between top and bottom electrode, or the difference in area.

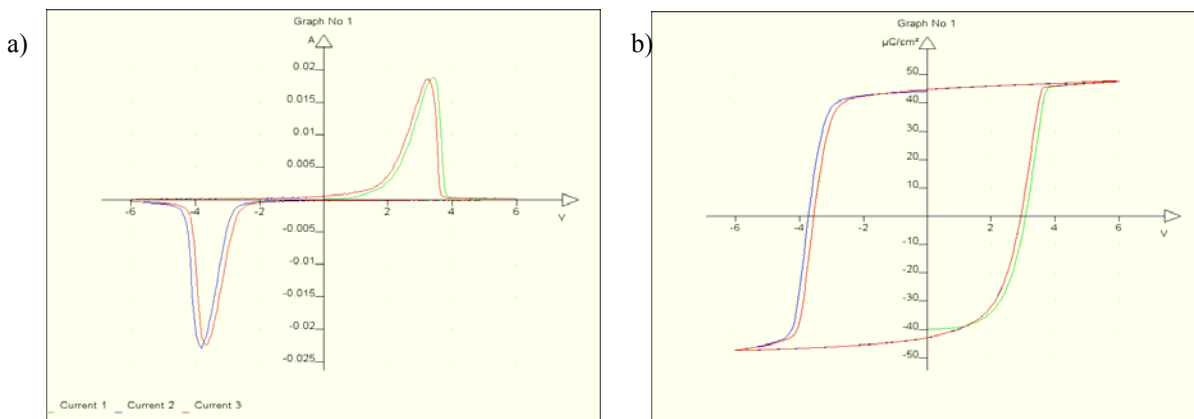


Figure 4-10 Macroscopic ferroelectric measurements of the sample a) current response b) polarization response that was calculated from the current response

4.5.3 PSTM measurements

Measurements of the piezoelectric activity by PSTM were done, see Figure 4-11. The voltage was gradually turned up from 0.5 V at the bottom to 6 V at the top. A frequency doubling is visible at 3 V.

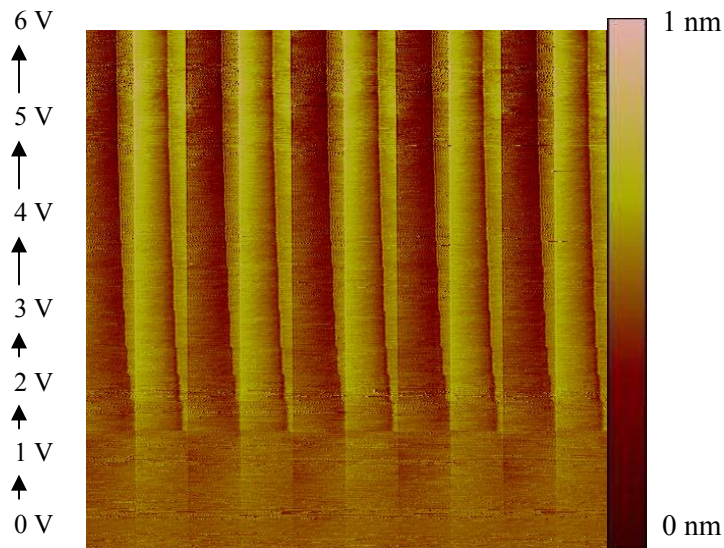


Figure 4-11 PSTM-image with piezoelectric deformations of the surface. Amplitude of the applied voltage was gradually turned up from 0.5 V (top) to 6 V (bottom)

The frequency of the triangular bias voltage on the sample was adjusted to the scanning rate of the STM. In this image the scanning rate is 2 Hz, which means the STM makes a trace and a retrace in 0.5 second. Only the trace is used to construct the image and takes 0.25 second. The applied voltage was set to be 21.735 Hz, to generate straight deformations exactly perpendicular to the horizontal scan lines. This results in 5 cycles of piezoelectric deformation per scan line.

By making a cross-section of the STM-image, the height profile can be generated. The height profile of multiple scan lines can be averaged to decrease the noise. This was done for scan lines that were generated by a constant voltage, for example only the 6 V area in Figure 4-12. This image shows that if the frequency of the applied sawtooth voltage was not tuned accurately with 4 decimals, the deformations not to appear perpendicular in the PSTM-image.

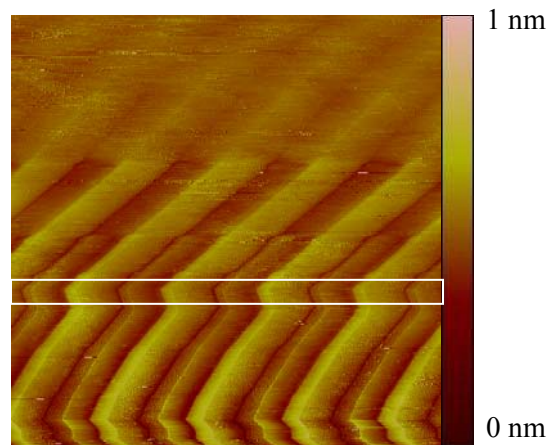


Figure 4-12 PSTM-image of with a rotating box located in the area that was generated by a single value (6V) of applied voltage, to calculate the height profile

Subsequently the height profile was divided by the applied voltage with sawtooth shape (Figure 4-13a). The butterfly loop was constructed (Figure 4-13c) by plotting the displacement Δz as a function of the voltage. The slope of the butterfly gives the piezoelectric constant (Figure 4-13d):

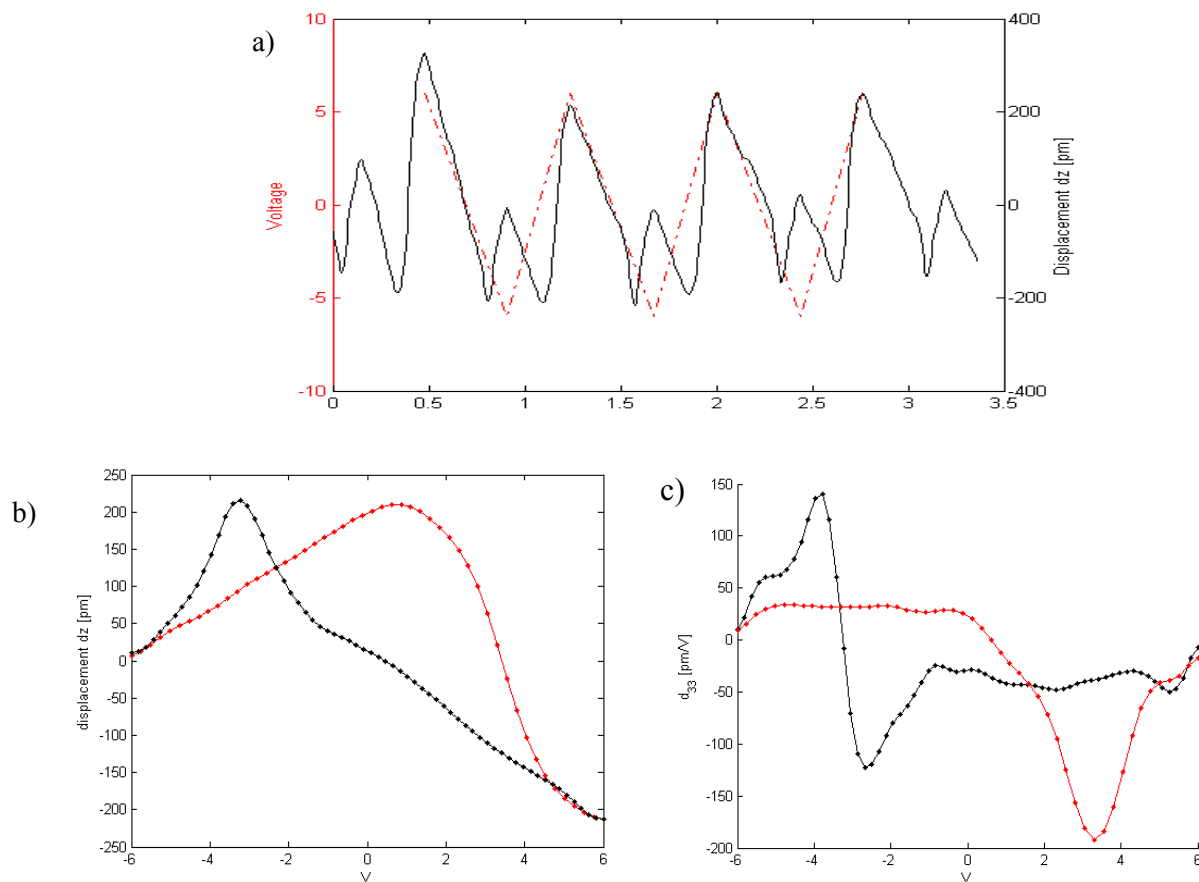


Figure 4-13 Piezoresponse measurements a) Height profile, which represents displacement as a function of time and applied triangular voltage b) d-E loop, displacement as a function of voltage c) Piezoelectric coefficient d_{33} as a function of voltage

The piezoelectric coefficient is determined from the slope of the butterfly-loop and is roughly 40 ± 10 pm/V. This value is comparable to values found in literature values for thin-film epitaxial PZT (52/48). Furthermore, an asymmetry in the d-E loop was observed. In Figure 4-13b, the switching at the positive coercive voltage occurs over a wider range of voltages than for the negative coercive voltage. This asymmetry was observed in the polarization measurements in Figure 4-10 as well. From this data this asymmetry seems more pronounced in the d-E loop than in the P-E loop.

Furthermore around the switching voltage, the piezoelectric constant shows a peak and is significantly higher than 40 pm/V. Operation of a device near the coercive voltage could possibly make use of this sudden switch of deformation.

From the d-E loop the best operation voltages for devices based on piezoelectric materials can be recognized. The regime with a stable constant slope should be used. The voltage should be kept under the coercive voltage ± 2.5 V for this device to avoid switching the material. The high piezoelectric constant at the switching voltages may also be interesting for applications.

4.5.4 Effects in the PSTM measurements

The PSTM has shown differences in the shape of the height profile, d-E loop and d_{33} -E loop. Over subsequent measurements the piezoresponse showed changes in magnitude and shape. Three possible effects for these differences can be imagined:

- Non-homogeneous materials properties
- Environmental effects
- Electrical effects

The non-homogeneous material properties are the possible domain structure in the PZT-layer causing local differences of the piezoelectric constant or elastic properties of the SRO generate a distortion of the displacement of the top layer. Furthermore the piezoelectric deformation may be change toward the edges of the electrodes, due to changing stress relaxation in the film. The first two PSTM studies mentioned local variations of the local piezoelectric constant for non-perovskites²⁸. Winters concluded that the observed variations in piezoelectric coefficient cannot be explained by spatial variations of the surface characteristics and is due to intrinsic properties of the tunneling contact under ambient conditions³², by using a configuration consisting of a double piezoelectric layer. To verify this, local variations of the butterfly loop are determined by 4 measurements on arbitrary points on the 1mm² top electrode. Little or no local variations were observed in Figure 4-14, meaning the top electrode moves up and down as can be expected from the piezoresponse of an ideal capacitor configuration in equation 4.2:

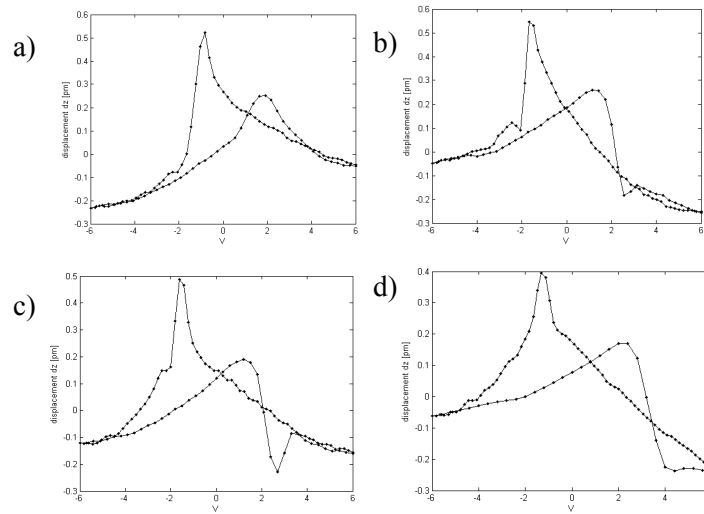
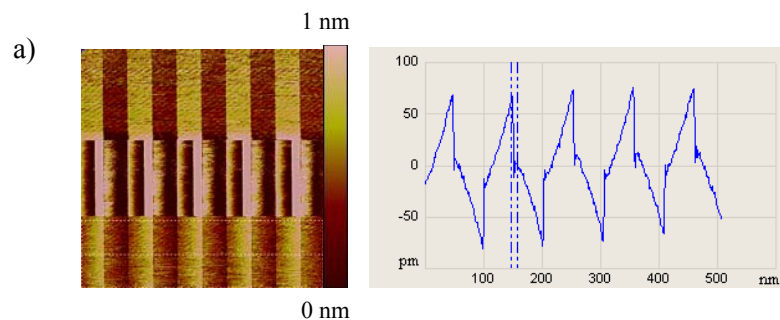


Figure 4-14 A d-E loop, measured on 4 arbitrary spots on the 1 mm² top electrode of the sample

Environmental effects can be caused by conditions such as the quality of the tip, dirt of water on the sample surface, atmospheric humidity or mechanical vibrations. Careful control over all these parameters is needed to obtain reproducible results. However detailed control of all these conditions is not possible.

Electrical effects may cause a substantial part of the deviations that occur in the height profiles. The following measurement is used to interpret the electrical effects. An extreme case was measured in Figure 4-15. The piezoresponse during one scan for a bias voltage that is subsequently 1.5 V, 6 V and 1.5 V again. Each height profile is calculated from the cross-section shown next to it, subsequently the lower part, the middle part and the upper part. It can be seen that the piezoresponse is completely different for each part.



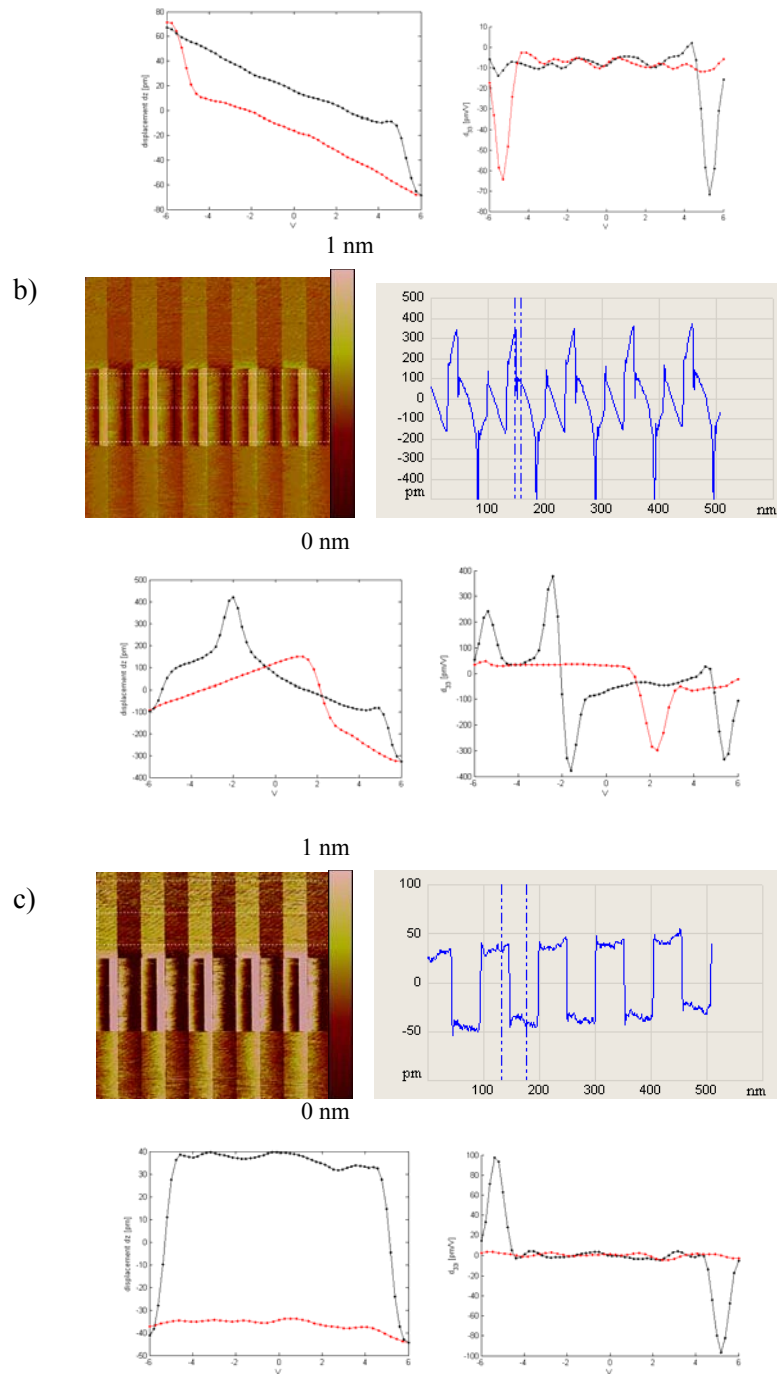


Figure 4-15 PSTM-image with three subsequent cross-sections, made by a) 1.5 V, b) 6V and c) 1.5V

The electrical effects can be explained by cross-talk between the electrical bias of the sample and the tunneling current of the STM. Since the electrical cross-talk seems to depend on the gradient of the applied voltage $\frac{dV}{dt}$, as can be seen in Figure 4-15c, the following mechanism is proposed. The constant switching of the material can cause the surface charge to accumulate and change the effective voltage over the plates. Especially in case of bad grounding an effective resistance to the ground appears R_{ground} , see the sample configuration in Figure 4-16. The capacitive current is:

$$I_{cap} \sim C \frac{dV}{dt} \quad (4.4)$$

Where I_{cap} is the resulting current, C is the capacitance and $\frac{dV}{dt}$ the gradient of the applied voltage.

This current leads to a shift of the potential of the electrodes. The bias on the electrodes can have a magnitude that is deviating from the value it was biased to. It can be noted that only Birk²⁸ noted an electrostatic effect during measurement of the piezoelectric constant of polymers. Now Figure 4-15 is interpreted as follows: in a) the piezoelectric effect and the cross-talk effect are equally in magnitude and added to give the height profile, in b) the bias is increased above the coercive voltage and piezoelectric switching appears, and in c) the piezoresponse contribution is lost and only the cross-talk effect is present.

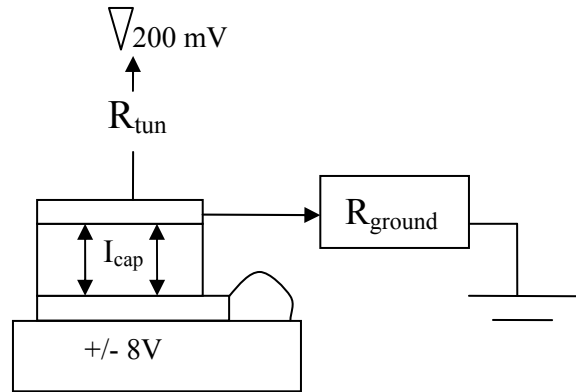


Figure 4-16 Schematical representation of the system, explaining effects of electrical cross-talk. I_{cap} is current through capacitive behavior, R_{ground} the resistance of the grounding and R_{tun} the resistance of the tunneling contact.

A model to study the consequences of this effect was constructed. It should be noted that not all measurements could be fit to a model exactly, but some major features will show to fit the model. A sawtooth voltage is constructed, see the dotted blue line. The applied bias has an amplitude of 6V and has an equilibrium value of 0V (dotted red line). Subsequently the piezoresponse (solid black line) is calculated, using a piezoelectric constant equal to 1. The coercive voltages are -3V (green line) and +3V (blue line), in this case. Each time an upward or downward straight line of the sawtooth-bias crosses a coercive voltage for the second time, the polarization of the sample switches, and the piezoelectric constant will be change sign and piezoelectric deformation Δz makes a jump and switches sign as well. Also the d-E loop was calculated, and shows a symmetric behavior around $V=0$. The d_{33} hysteresis loop was deduced from it. The peaks at the outer edges are an artifact of the model due to a reversal of the voltage and the peaks of the switching can be clearly seen. When comparing Figure 4-17c to measurements in Figure 4-13d, these peaks can be recognized. One peak in the measurements is not represented in the model and may be attributed to an overshoot effect of the STM.

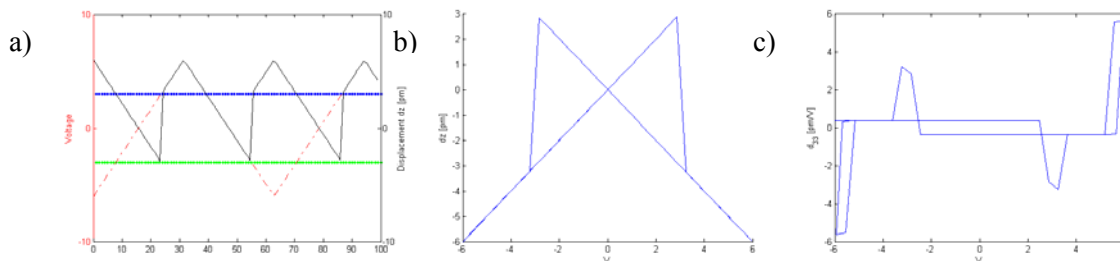


Figure 4-17 a) Applied bias with amplitude 6V and piezoresponse as a function of time, and b) d-E loop calculated from this. The coercive voltage is -3V and +3V c) the d_{33} loop.

An additional bias of the top electrode will be entered in the model. According to equation 4.4, in case $\frac{dV}{dt} > 0$, an arbitrary value of 1 pm is added to the piezo response and in case $\frac{dV}{dt} < 0$, the same arbitrary value of 1 pm is subtracted from the piezoresponse. This results in an asymmetric loop, with its peaks shifted vertically. This plot resembles Figure 4-15, and also Figure 4-14. Furthermore, the asymmetric behavior will vanish in the plot of the piezoelectric constant d_{33} , as shown in Figure 4-18c, which is similar to Figure 4-17c (except for the artifact at the edges). Only an additional peak at the outer edges of this plot will occur, but this does not interfere with the measurement of the value of d_{33} . This means the determining the piezoelectric constant is not harmed by this electrical effect. Keeping this conclusion in mind, height profile in Figure 4-15b looks chaotic at first glance, but can be used to determine the piezoelectric constant. The value is 40 ± 10 pm/V and agrees to a previous measurement in Figure 4-13b.

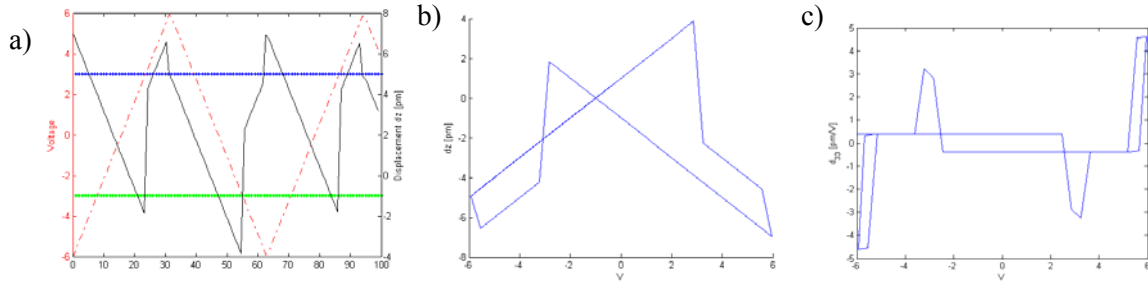


Figure 4-18 Applied bias with amplitude 6V and piezoresponse as a function of time, where if $dV/dt > 0$ 1pm is added to the piezoresponse and if $dV/dt < 0$ 1pm is subtracted from the piezo response and b) d-E loop that was calculated from this and c) the d_{33} loop.

4.6 Spectroscopic PSTM

This paragraph describes the efforts on PSTM measurement made in with the STM in spectroscopic mode. First the principle of operation will be described, followed by the experimental setup and results.

4.6.1 Principle of operation

Spectroscopic STM is a technique widely used to determine the density of states of materials. It means the feedback of the STM is put off while the tunneling current is measured as a function of the applied voltage between tip and sample. Furthermore the tunneling current as a function of the tip-sample distance has been used to measure the vibrations of single molecules. The use of the exponential tunneling current for quantitative measurements of the piezoelectric deformations of surfaces (spectroscopic PSTM) has not been investigated.

The relation for the exponential tunneling current as a function of distance is:

$$i = c \frac{V}{s} e^{-2\kappa s} \quad (4.5)$$

with I the tunneling current, V the bias voltage between tip and sample and s the tip-sample distance. In this case the density of states is not expected to influence the tunneling current.

In case a ferroelectric sample that is biased by a voltage on its electrodes, a butterfly loop (d-E loop) is expected. However, the exponential relationship between the current and the tip-sample distance is still in the data. An ideal piezoresponse loop was calculated by the model, showing displacement as a function of voltage. The plot was inverted, since the sample displacement and the tip-sample distance follow the relation:

$$x = -s \quad (4.6)$$

Subsequently the exponential relation 4.4 was inserted in the model, to calculate the tunneling current as a function of voltage. Figure 4-19 shows two butterfly loops with on the vertical axis the displacement in Figure 4-19a and the tunneling current Figure 4-19b.

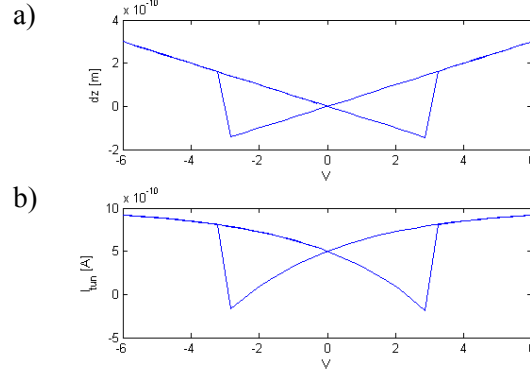


Figure 4-19 Model showing expected a) displacement and b) the tunneling current as a function of applied voltage to the sample

It is not possible to obtain the piezoelectric coefficient from this plot, since the exponential tunneling current and the distance are linked by an unknown constant, see equation 4.5. However, a relative indication of the displacement can be given by calculating the logarithm of the tunneling relation:

$$\ln i = \ln c \frac{V}{s} - 2\kappa s \quad (4.7)$$

The first term on the right side is negligible, since $c \frac{V}{s} \approx 10^{-10}$ and $\ln c \frac{V}{s} \approx \ln 10^{-10} \approx 0$. The ultimate relation between the tip-sample distance and the tunneling current is:

$$s = -\frac{1}{2\kappa} \ln i \quad (4.8)$$

When taking the logarithm of the current, the tip sample distance can be obtained (only the shape not magnitude): butterfly-loop. This should be inverted to get the displacement with positive value upward.

To extract a quantitative number for the piezoelectric constant, a different derivation should be done. This is based on using the exponential relationship. The slope of the i-V loop can be used to obtain the piezoelectric coefficient d_{33} , using the course of the exponential decay. The following expressions describe a differential equation between current I and tip-sample distance s:

$$\frac{di}{ds} = \frac{i}{s} - 2\kappa i \quad (4.9)$$

The first term equation 4.10 can be neglected, since $\frac{i}{s} \approx \frac{100 \text{ pA}}{1 \text{ nm}} \approx 0.1 \text{ pA/nm}$ is far smaller than the last term in equation 4.10: $2\kappa i \approx 2 \cdot \frac{20}{\text{nm}} \cdot 100 \text{ pA} \approx 4000 \frac{\text{pA}}{\text{nm}}$. The resulting equation is:

$$\frac{di}{ds} = -2\kappa i \quad (4.10)$$

A linear relationship between displacement and V is assumed and can be inserted into the differential equation 4.11:

$$s = \pm d_{33} \cdot V \quad (4.11)$$

$$\frac{di}{d(d_{33} \cdot V)} = 2\kappa i \quad (4.12)$$

$$\frac{di}{dV} = -2\kappa d_{33} i \quad (4.13)$$

The exponential decay is determined by the value of $\kappa \approx 2\text{\AA}^{-1}$. Finally, the d_{33} can be determined by plotting the following relation and determining the derivative:

$$\left(\frac{1}{-2\kappa i} \right) \frac{di}{dV} \text{ versus } V \quad (4.14)$$

4.6.2 Experimental setup

The same experimental setup as for the PSTM measurements in feedback mode has been used, consisting of the sample, sample holder and Multimode Microscope. The Nanoscope software allows for measurement of ramp plots, where one parameter can be chosen to vary while the tunneling current is measured. In this case, by keeping the tip at a constant height, the tunneling current will depend on the tip-sample distance. The voltage on the bottom electrode will induce a sample deformation. The configuration is shown in Figure 4-20:

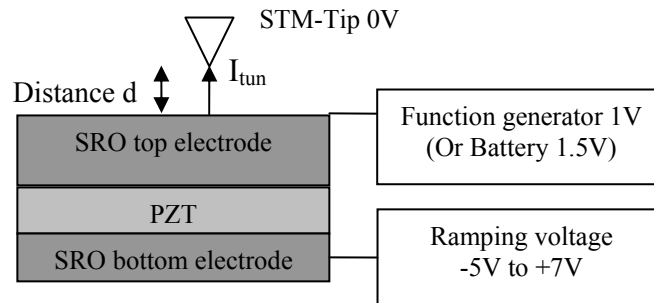


Figure 4-20 Schematic configuration for spectroscopic PSTM

In this option, the STM-tip should be engaged while the system operates in feedback mode. Standard parameters such as current setpoint and bias need to be adjusted. Subsequently a single ramp can be done by switching off the feedback and do the ramp of the voltage. After measurement the system goes into feedback state again. It should be noted that continuous ramping is also possible. In that case the system does not switch back to feedback operation state after finishing the ramp. This feedback determines starting point of the ramp and thus the level of the tunneling current for the ramp. Since the STM is a low-current STM, it turned out that the upper limit to the current was only $\pm 1\text{nA}$.

In the spectroscopic mode, the voltage of the tip is automatically set to 0 V. Therefore the top electrode was biased to create a voltage between the tip and sample. The bias was applied by a dc-voltage generator. This

has shown to supply a small voltage wrinkle on the voltage signal, which interferes with the STM tunneling current. Therefore a battery of 1.5 V can be recommended, since this is a more stable DC-voltage-source.

The speed of the ramp is important since drift can corrupt the measurements at slow speeds. Ramping thus should be done at 1Hz or more, which generates total ramping time of 2 seconds or less (for a trace and a retrace).

Table 4-1 Settings for spectroscopic PSTM

Frequency	2 Hz
Bias	1050 mV
Current setpoint	200 pA
Current limit	2 nA
Proportional gain	0.5
Integral gain	0.5

4.6.3 Results



Figure 4-21 Tunneling current as a function of applied voltage to the sample, two data sets

This expression was used to plot the tip-sample distance as a function of applied voltage to the sample. This data was smoothed to reduce the noise, see Figure 4-22:

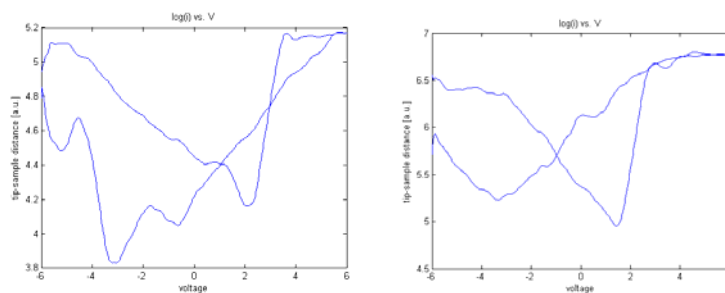


Figure 4-22 Tip-sample distance as a function of applied voltage to the sample, two data sets

Figure 4-23 shows this plot. A large amount of noise is present in the data. A linear fit of the slope gives the d_{33} . This fit should be applied only to a part of the data which is linear.

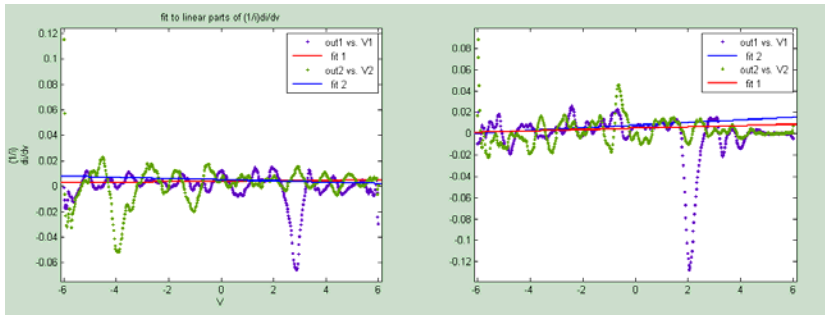


Figure 4-23 Piezoelectric constant as a function of voltage measured by spectroscopic PSTM, two data sets

The slope to the linear parts of Figure 4-23 can be obtained using a linear fit and are presented in Table 4-2. The piezoelectric coefficient can be determined, using $\kappa = 20 \cdot 10^{-3} \text{ pm}^{-1}$ and relation:

$$d_{33} = -\frac{P_1}{2\kappa} \quad (4.15)$$

Table 4-2 Slope of the linear parts of Figure 4-23, two data sets

	slope left [V ⁻¹]:	D ₃₃ [pm/V]	slope right [V ⁻¹]:	D ₃₃ [pm/V]
Fit 1	1.626e-4	0.04065	1.174e-3	0.02935
Fit 2	-4.804e-3	0.1201	-4.62e-4	0.01155

The piezoelectric coefficient does not agree to the literature value for epitaxially PZT thin films, which is 50 pm/V. A conclusion is that the exponential decay is not sufficiently pronounced in the data to determine the piezoelectric constant. The same measurements explained above were done with the STM in normal operation, without the PicoAmp Boost Box. Currents in the range up to 200nA could be measured. No improvement of the calculated d_{33} was observed.

Improvements to the measurements can be made using multiple scan lines. The above data were acquired using a single ramp. In general, AFM and STM use the capability of doing continuous scanning and using flattening functions to improve the data. In principle, continuous ramping can be done here as well. Acquiring multiple loops allows for averaging the response and thus reducing the noise. The Nanoscope option Continuous Image Tunneling Spectroscopy (CITS) can possibly be used for this.

Conclusions and recommendations

The objective of this thesis was the exploration of the use of scanning probe techniques for characterization of properties of piezoelectric and ferroelectric thin films. In this thesis, both Piezo Force Microscopy (PFM) and Piezo Scanning Tunneling Microscopy (PSTM) have been investigated. The operation principle, sensitivity and reliability of these techniques have been evaluated. Furthermore the measurement system and operating parameters have been presented.

Investigations of piezoresponse are based on the inverse piezoelectric effect, which means a surface deformation is generated by an electric field. Some characterization methods can yield only qualitatively measurements, meaning the magnitude of the piezoelectric response cannot be determined exactly. In this thesis, efforts have been made to do quantitative measurements. To do the measurements, a sample was fabricated consisting of a STO substrate, a 50 nm SRO bottom electrode, a 100 nm – (001) PZT (52/48) piezoelectric film and in case of the PSTM measurements a 50 nm top electrode of SRO.

PFM was described by the basic principles, experimental conditions and results that were obtained. PFM is suitable for imaging of surface polarization of ferroelectric films. It can give information on the local polarization and is able to control local polarization by ferroelectric lithography. Using this method, the characters ‘IMS’ with a diameter of 2 μm , were written on the surface, by polarization of the surface. These results are only qualitative, due to two kind difficulties in quantifying the piezoelectric coefficient. Firstly, the conductive probe used in PFM generates an inhomogeneous electric field. A model was presented to discuss this and show that no exact knowledge about the electric field can be obtained. Furthermore the tip-sample interaction is very complex, since electrostatic effects influence the deflection of the tip. Degradation of the tip and the formation of a ‘dead layer’ on the surface have shown to limit the tip-sample interaction. The PFM technique can be applied to all piezoelectric materials with a conducting bottom electrode, but the technique needs accurate tuning of the parameters to the material.

The use of a STM promises high accuracy measurements of surface deformation, since it uses the exponential tunneling current as a function of the tip-sample distance. To avoid the non-linear field in the material, the sample configuration was extended with a top electrode, to form an ideal capacitor with a linear electric field between its electrodes. In this thesis, the PSTM technique was described by the basic principles, experimental conditions and results that were obtained. The applied voltage on the film of maximal 8 V for PZT sample has shown to generate piezoelectric deformations in the order of 50 to 500 pm. In optimal operating conditions, the STM has shown a sensitivity of 10 pm.

From the PSTM-images, height profiles can be deduced by taking a cross-section of the image. The deformation as a function of the voltage, also known as the ‘butterfly’ loop, was calculated from the height profile. An asymmetry was observed that was probably caused by electrode effects. This asymmetry was also observed in macroscopic polarization measurement. The slope of this loop gives the longitudinal piezoelectric coefficient d_{33} of the PZT (52/48) has shown to be $40 \pm 10 \text{ pm/V}$, which agrees with literature values. These plots agree to the results obtained by Kuffer et al³⁰. Near the coercive voltage a spike in the d_{33} was obtained, due to the sudden reversal of the sample deformation by the ferroelectric switching. The resulting d_{33} have shown to be reproducible, indicating a reliable technique.

The PSTM technique has shown to be easy to implement on a standard STM system. A special sample holder was constructed to allow easy electrical connection by bonding wires to both the top and bottom electrode. In this way the biasing voltage or grounding can be applied to the sample from any source. The frequency of the applied voltage should be low enough to assure proper feedback operation of the STM. The noise in the system has shown to limit the resolution. Furthermore, the shapes of the height profiles showed the influence of some external effects. Especially electrical effects have shown to influence the height profiles which means proper grounding of the top electrode is important. No local differences in the piezoelectric constant were observed. In an effort to understand the piezoresponse behavior, the influences

were simulated by a simple model. This has shown that the electrical effect is proportional to the gradient of the applied voltage and does not influence the measurement of the piezoelectric constant.

Spectroscopic PSTM measurements have been explored, in order to determine the piezoelectric coefficient. By keeping the tip at a constant height, the tunneling current can be measured as a function of the surface deformation, which is induced by an applied voltage. Spectroscopic STM only allows useful data to be obtained from relative measurements of the tunneling current. Therefore the exponential decay in the tunneling current signal was used to plot the numerical derivative of the current as a function of V and calculate the slope. Piezoelectric constants were obtained that were far lower than the literature value, meaning the technique needs some adjustments. Some recommendations on this technique are discussed below.

PSTM has shown to be the most powerful technique to obtain values for the d_{33} . PFM has too many uncertainties in applied field and geometry and the spectroscopic PSTM did not show the expected exponential dependence as a function of the piezoelectric deformation.

Recommendations

PFM is a technique which has been used for a number of years. It is known that the spring constant of the cantilever should be higher than 10 N/m to assure predominantly electromechanical piezoelectric response. This was confirmed by measurements. The tip is prone to degradation, due to high force on the tip or high voltage on the tip. Furthermore the samples have shown to degrade rapidly, due to the formation of a 'dead layer' by collection of dust and water and chemical reactions. It is recommended to use freshly fabricated samples and in case of storing they should be stored in vacuum. The ferroelectric lithography can be used to polarize feature of the diameter of the tip, which is in the order of 20 nm.

PSTM has shown resolution of down to 10 pm under ideal conditions. As was described before the operation of the PSTM method is very sensitive to external conditions (like any other scanning probe technique). The sample needs to be mounted on the sample holder solidly, to avoid unwanted movements. The noise is a limiting factor for the resolution and efforts can be made to find the major noise source and improve it. An indication could be to use better quality electrical cables, better electromagnetic shielding or better vibration reduction. A decrease of the floating bias or charging effects will lead to more steady shaped height profiles and results will be better reproducible. Furthermore the analysis using PSTM is ready to be extended to other materials, which have for example a smaller piezoelectric coefficient and different hysteresis behavior. One should keep in mind conditions such as the use of top and bottom electrodes is needed and the piezoelectric material should be insulating.

Spectroscopic STM needs more efforts to do measurements in a larger current range by increasing the current limit. This will allow the exponential decay to be more pronounced and better determining of the piezoelectric constant will be able. Furthermore multiple ramping has to be explored, so that noise or local errors can be reduced. The option Continuous Image Tunneling Spectroscopy (CITS) in Nanoscope software shows possibilities for this. It should be noted that continuous ramping has strongly shown charging effects to occur.

Dankwoord

Graag wil ik van deze gelegenheid gebruik maken om mensen te bedanken die mijn studietijd en het afstuderen veel leuker hebben gemaakt, en zonder wie het sowieso onmogelijk zou zijn geweest om deze prachtige tijd te volbrengen.

Allereerst wil ik de vakgroep Inorganic Materials Science bedanken voor de afgelopen 9 maanden. Het is absoluut de leukste en sociaalste vakgroep van het gebouw Hogekamp, op zowel op inhoudelijk als sociaal vlak (nee, ik ben helemaal niet bevooroordeeld...)! Natuurlijk wil ik Paul bedanken als dagelijkse begeleider. Het was goed samenwerken, ik heb veel van je opgestoken, en bedankt voor alle hulp bij het verslag en de berg samples, als ik ze weer eens had laten doorbranden. Guus voor de begeleiding en het bewaken van de juiste richting van het werk, en Dave voor al je vertrouwen en gastvrijheid in de afgelopen maanden. Ook Harold Zandvliet wil ik bedanken voor een aantal leuke ideeën tijdens deze afstudeerperiode.

Natuurlijk alle andere groepsleden, ik kan ze niet allemaal bij naam noemen, en technische begeleiding voor de gezelligheid tijdens de koffiepauzes, de fantastische studiereis, uitjes en de partijtjes voetbal. Verder wil ik graag alle medeafstudeerders en andersoortige kamergenoten bedanken voor de melige grappen en verscheidenheid aan gespreksonderwerpen die de boel opfristen als het werk wat 'lauw' dreigde te worden. Studiegenoten in alle soorten en maten wil ik bedanken, in het bijzonder mijn bestuursgenootjes en de Brazilië-gangers van de studiereis en projectgenoten. Voor de Novaselic-bandmaatjes, hopelijk ligt er nog een nieuwe cd in het verschiet, so let's rock on. Uiteraard ook veel dank aan de vriendengroep van thuis, voor het plezier waarmee het toch altijd een genot blijft om menig avondje tot de late uurtjes door te laten gaan.

Mijn ouders wil ik heel hartelijk bedanken voor alle steun, dat jullie altijd voor me klaar stonden en me de kans geven om mezelf te ontwikkelen en Natascha, dat je er altijd voor me was. Met jou aan mijn zij waren de afgelopen jaren vele malen leuker.

Zo, nu eerst ff op vakantie, ik wens iedereen veel plezier met werken! En aan alle mede-AFM'ers: jullie hebben weer de ruimte want deze AFM-terrorist is eindelijk weg!

Ruud Steenwelle
14 September 2007

References

- ¹ H. Ibach, H. Luth, Solid-state Physics, 3rd edition, Springer, 2003.
- ² J.C. Burfoot, Ferroelectrics, Princeton, New Jersey, 1967.
- ³ R.E. Newman, Properties of Materials, Oxford University Press, 2005.
- ⁴ R. Tilley, Understanding Solids, Wiley, 2004
- ⁵ D.J. Griffiths, Introduction to Electrodynamics, Prentice Hall New Jersey, 3rd edition, 1999
- ⁶ Piezoelectric Ceramics, Jaffe Cook Jaffe, Academic Press, 1971
- ⁷ C. Harnagea, Local piezoelectric response and domain structures in ferroelectric thin films investigated by voltage-modulated force microscopy, PhD thesis, 2001.
- ⁸ T. Ikeda, Fundamentals of Piezoelectricity, Oxford University Press, 1990.
- ⁹ G.W. Taylor, J.J. Gagnepain, T.R. Meeker, T. Nakamura, and L.A. Shuvalov, Piezoelectricity, Gordon and Breach Science Publishers, New York, 1985.
- ¹⁰ Kenji Uchino, Ferroelectric devices, Marcel Dekker, inc., 2000.
- ¹¹ Investigations of polarization switching over broad time and field domains in various ferroelectrics, Christelle Jullian, ??
- ¹² Piezoelectric Ceramics, Jaffe Cook Jaffe, Academic Press, 1971
- ¹³ M Dawber, Physics of thin-film ferroelectric oxides, Rev of Modern Physics, vol. 77, 1083, 2005.
- ¹⁴ C. Kittel, Introduction to Solid State Physics, 6th edition, Chapter 13, 1986.
- ¹⁵ Piezoelectric Ceramics, Jaffe Cook Jaffe, Academic Press, 1971
- ¹⁶ Xiao-Du, Jiehui Zheng, Uma Belegundu, and Kenji Uchino. Crystal orientation dependence of piezoelectric properties of lead zirconate titanate near the morphotropic phase boundary, Appl. Phys. Lett. 72, 19
- ¹⁷ C. Aruta, et. Al., Synchrotron X-ray diffraction study of SrRuO₃/SrTiO₃/SrRuO₃ nano-sized heterostructures grown by laser MBE, Eur. Phys. J. B, 2005
- ¹⁸ C.L. Jia, Lattice strain and lattice expansion of the SrRuO₃ layers in SrRuO₃ on PbZr_{0.52}Ti_{0.48}O₃ on SrRuO₃ multilayer thin films, Journal of Applied Phys, 92,1, 2002
- ¹⁹ Fourier analyse, college reader Analyse B, University Twente, 2002
- ²⁰ P.Paruch. T.Tybell. and J.-M. Triscone, Nanoscale control of ferroelectric polarization and domain size in epitaxial Pb(Zr_{0.2}Ti_{0.8})O₃ thin films, Appl Phys Lett 79, nr. 4, 2001.
- ²¹ T. Tybell, P. Paruch, T. Giamarchi, and J.-M. Triscone, Domain wall creep in epitaxial ferroelectric Pb(Zr_{0.2}Ti_{0.8})O₃ thin films, Cond. Matt. 0203381 v1, 2002
- ²² C. Harnagea and A. Pignolet, Challenges in the Analysis of the Local Piezoelectric Response, in Nanoscale Characterisation of Ferroelectric Materials, Scanning Probe Microscopy Approach, M. Alexe. A. Gruverman (Eds.), Springer, 2004
- ²³ P.M. Te Riele, Simulation of the electric field inside for a halve sphere above a conducting plate for interpretation in PFM, unpublished, 2006.
- ²⁴ Kalinin. S.V. and D.A. Bonnell, Electric Scanning Probe Imaging and Modification of Ferroelectric Surfaces, 2003.
- ²⁵ Kalinin. S.V., A decade of piezoresponse Force Microscopy, Progress, Challenges and Opportunities, IEEE Tuff, 2003.
- ²⁶ Zavala G., Fendler J.H., Trolier-McKinstry S., Characterization of ferroelectric lead zirconate titanate films by scanning force microscopy. J. Appl. Phys. 81, 7480, 1997.
- ²⁷ G. Binnig, H. Rohrer, Surface studies by scanning tunneling microscopy, Phys. Rev. Lett., 49, 57, 1982
- ²⁸ H. Birk et al., The local piezoelectric activity of thin polymer films observed by scanning tunneling microscopy, J. Vac. Sci. Technol. B 9(2), 1991.
- ²⁹ Veeco Digital Instruments Multimode Instruction Manual, version 4.31e, 1999.
- ³⁰ O. Kuffer, I. Maggio-Aprile, J.-M. Triscone, and O. Fischer, Piezo electric response of epitaxial Pb(Zr_{0.2}Ti_{0.8})O₃ films measured by scanning tunneling microscopy, Appl Phys Lett. 77, 11, 2000
- ³¹ S.N. Magonv, M. Whangbo, Surface Analysis with STM and AFM, VCH, 1996.
- ³² R. Winters et al. Measurement of the piezoelectric of films with scanning tunneling microscopy, J. Vac. Sci. Technol. B 13(3), 1995.